ELSEVIER

International Journal of Mass Spectrometry 217 (2002) 195–230

International Journal of Mass Spectrometry

www.elsevier.com/locate/ijms

Thermochemistry and unimolecular reactivity of protonated α,ω-aminoalcohols in the gas phase

Guy Bouchoux[a,*], Nadège Choret[a], Florence Berruyer-Penaud[b], Robert Flammang[c]

[a] *Laboratoire des Mécanismes Réactionnels, Département de Chimie, UMR CNRS 7651, Ecole Polytechnique, 91128 Palaiseau Cedex, France*

[b] *Laboratoire de Chimie Physique, Groupe de Chimie Théorique, UMR CNRS 8000, Bâtiment 490, Université Paris Sud, 91405 Orsay Cedex, France*

[c] *Laboratoire de Chimie Organique, Université de Mons-Hainaut, 20 Place du Parc, B-7000 Mons, Belgium*

Received 22 October 2001; accepted 15 December 2001

Dedicated to the memory of Pierre Longevialle, a missed dear friend and an inspired scientist.

Abstract

Competitive deamination and dehydration of protonated α,ω-aminoalcohols (1,2-aminoethanol (**1**), 1,3-aminopropanol (**2**), 1,4-aminobutanol (**3**) and 1,5-aminopentanol (**4**)) in the gas-phase has been examined by both tandem mass spectrometry experiments including metastable ions decompositions and collisional activation (CA) techniques and molecular orbital calculations. For all the precursor molecules **1**–**4**, CA experiments demonstrate that the low energy product ions are either a protonated cyclic amine or a protonated cyclic ether. The mechanisms of the internal nucleophilic substitution reactions leading to these products have been detailed at the MP2/6-31G* level of theory. The thermochemistry associated with the initial protonation process of **1**–**4** has been examined up to the G2(MP2,SVP) level. (Int J Mass Spectrom 217 (2002) 195–230)

Keywords: Protonated α,ω-aminoalcohols; Acid-catalyzed cyclization

1. Introduction

Pierre Longevialle has been interested by the processes occurring under the chemical ionization conditions since the birth of this technique. In the 1970s, he observed that the loss of water from protonated steroidal aminoalcohols is intense only if the distance between the oxygen and the nitrogen is too large to allow the formation of an internal hydrogen bond [1]. Latter, the availability of a series of α,β-aminoalcohols with constrained geometry has been then the starting point of several studies aiming to quantify these observations [2–6]. In a first paper, Pierre shows clearly that the amount of water elimination from the $[MH]^+$ ions increases when the dihedral angle OCCN increases. He explains this phenomenon by the formation of a strong internal hydrogen bond in the N-protonated forms at small dihedral angle preventing the formation of a significant proportion of the O-protonated form, which, obviously, is at the origin of the water loss. This view has been corroborated by the measurement of the gas-phase basicity of the considered α,β-aminoalcohols [4] and by the examination of the

* Corresponding author.
E-mail: bouchoux@dcmr.polytechnique.fr

1387-3806/02/$ – see front matter
PII S1387-3806(02)00577-8

incidence of the protonation exoergicity upon water loss [6].

Further, the role of the O···N distance in the decomposition of protonated aminoalcohols has been evidenced in other series [7–13]. For example, it has been established that the protonated aliphatic α,ω-aminoalcohols eliminate competitively H_2O and NH_3 in a ratio which show large variations as a function of the chain length and of the internal energy content of the dissociating species. Surprisingly enough, the structure of the fragment ion has not been characterized in the course of these studies. In fact, a cyclic structure has been assumed and supported by an argumentation based on the comparison of product ions stability. However, recent data show that the cyclic ions are not always the most stable. Moreover, for such internal cyclization processes, strain energies could be important and critical energies may dramatically differ from reaction enthalpy. This has been recently established for protonated diols [14] and protonated diamines [15] and, therefore, has to be expected for aminoalcohols.

The goal of the present study is to examine, both experimentally and theoretically, the behavior of the four simplest α,ω-aminoalcohols: 1,2-aminoethanol (**1**), 1,3-aminopropanol (**2**), 1,4-aminobutanol (**3**), and 1,5-aminopentanol (**4**). By analogy with the homologous diols and diamines, the losses of H_2O and NH_3 from protonated α,ω-aminoalcohols are expected to lead, either, to protonated cyclic amine or ether by intramolecular nucleophilic substitution (channels a_1 and a_2, Scheme 1), or, to protonated imine or aldehyde by internal hydride ion transfer (channel b_1 and b_2, Scheme 1).

Tandem mass spectrometry experiments, and particularly, collisional activation (CA), has been used to characterize the structure of the ionic products of the dehydration and deamination reactions. For this purpose, collisional experiments were conducted on the dissociation products of protonated molecules **1**–**4** in a six sectors magnetic instrument. On the other hand, the potential energy profile of each reaction path has been investigated at the MP2/6-31G(d) level of theory in order to understand the experimental observations.

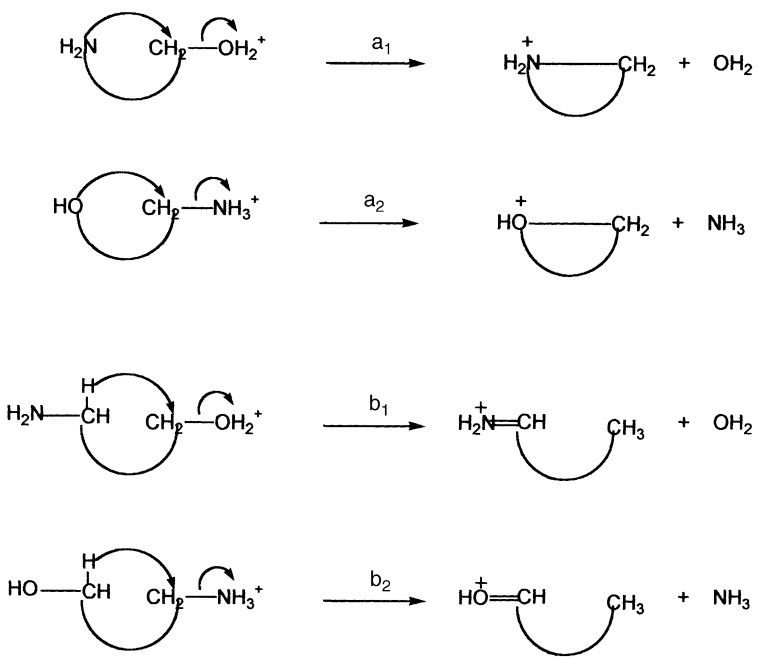

Scheme 1.

Finally, the protonation thermochemistry has been examined up to the G2(MP2,SVP) level after conformational analysis of α,ω-aminoalcohols **1**–**3** and their protonated forms.

2. Experimental and computational

The reactions of metastable protonated aminoalcohols **1**–**4** were studied with a VG-ZAB-2F double focusing mass spectrometer (B-E) operating in the chemical ionization mode using methanol as reagent gas. The accelerating voltage was set at 8 kV, the electron energy at 150 eV and the emission current at 0.5 mA. The source temperature was kept at 180 °C. The mass analyzed ion kinetic energy (MIKE) spectra of metastable ions were obtained, as usual, by selecting with the magnet the ion to be studied and scanning the electrostatic analyzer voltage. The kinetic energy release distribution has been derived from the analysis of the metastable peak profile using the method described in [16].

The collisional experiments were carried out with a VG-Analytical Auto Spec-6F mass spectrometer ($E_1B_1E_2$–$E_3B_2E_4$) [17] operating in the chemical ionization mode using methanol as reagent gas. The accelerating voltage was set at 8 kV, the electron energy at 70 eV and the emission current at 1 mA. The source and the septum inlet temperatures were 200 and 160 °C, respectively. For the experiments using helium as target gas, the ions of interest were selected by E_1B_1 and subjected to CA with helium in the third field-free region (FFR) of the instrument; the helium pressure was adjusted in order to reduce the signal to ca. 70% of its original value. The fragments were then analyzed by scanning E_2 and detected by the off-axis detector located in the fourth FFR. The CA (O_2) spectra were obtained in a similar way by selection of the ions with $E_1B_1E_2$ and CA with dioxygen in a gas cell located in the fourth FFR, the fragments were analyzed with E_3 and detected by the off-axis detector located in the fifth FFR. During the MS/MS/MS experiments, the ions produced in the third FFR by dissociation of a precursor selected by E_1B_1 are further selected by E_2 and subjected to CA with O_2 in the gas cell situated before E_3; the fragments are analyzed by scanning E_3. The CA spectra presented in Tables 2, 4, 6 and 8 are the result of ≈30 signal accumulations. The chemical samples are commercial compounds (Aldrich Chemical) of research grade; high purity gas were used in the collision experiments: helium 5.0, oxygen 2.6, nitrogen 5.0.

Standard ab initio molecular orbital calculations have been carried out using the Gaussian-98 series of programs [18]. The geometries of the different species investigated were first optimized at the HF/6-31G* level and then refined at the MP2(FrozenCore)/6-31G* level to take electron correlation effects explicitly into account. The zero-point energy (ZPE) has been calculated at the latter level and scaled by a factor 0.967 [19]. This procedure has been used during the exploration of the potential energy profiles associated with the dissociations of protonated molecules **1**–**3**. It has been established that accurate heats of formation (i.e., $\pm 6\,\mathrm{kJ\,mol^{-1}}$) can be obtained from calculations at the G2 level of theory [20a,20d] or its variants, G2(MP2) [20b,20d] and G2(MP2,SVP) [20c,20d]. In the present study, heats of formation have been evaluated from the G2(MP2) total energies by considering the atomization reactions [20e]. Using this approach, the heat of formation at 0 K for a given species X, $\Delta_f H_0^\circ(\mathrm{X})$, is given by

$$\Delta_f H_0^\circ(\mathrm{X}) = \sum \Delta_f H_0^\circ(\text{atoms}) - \sum E[\mathrm{G2(MP2,\,SVP)}](\text{atoms}) + E[\mathrm{G2(MP2,\,SVP)}](\mathrm{X}) \quad (1)$$

with $E[\mathrm{G2(MP2)}] = -0.5$, -37.78432, -54.51798 and -99.63282 Hartree for the H, C, N, and O atoms, respectively. The heat of formation at 298 K is therefore, given by

$$\Delta_f H_{298}^\circ(\mathrm{X}) = \Delta_f H_0^\circ(\mathrm{X}) + \Delta_{298} H^\circ(\mathrm{X}) - \sum \Delta_{298} H^\circ(\text{elements}) \quad (2)$$

where the difference between the enthalpy at 298 and 0 K is represented by the terms $\Delta_{298}H^{\circ}(\Delta_{298}H^{\circ} = H^{\circ}_{298} - H^{\circ}_{0})$. For the elements, experimental $\Delta_{298}H^{\circ}$ values have been used (i.e., 8.468, 1.050, 8.669 and 8.680 kJ mol^{-1} for $H_{2(g)}$, $C_{(s)}$, $N_{2(g)}$ and $O_{2(g)}$, respectively), whereas, for the other species, the translational and rotational contributions were taken equal to 3*RT* and the vibrational contribution estimated from the scaled (by a factor 0.893) HF/6-31G(d) vibrational frequencies.

3. Results and discussion

A summary of the relevant thermochemistry of the protonated α,ω-aminoalcohols **1**–**4** and their possible dissociation products is given in Table 1.

The data reported in Table 1 are essentially of experimental origin, the only exceptions are the protonated aminoalcohols themselves. For the latter, we used the 298 K heats of formation deduced from atomization energies calculated at the G2(MP2) level. Accordingly, no experimental value of the heat of formation of neutral aminoalcohols is available, the few tabulated values [21] are in fact estimates based on group additivity method [22]. It constitutes, at best, upper limits since this method does not take into account the possibility of internal hydrogen bond. Furthermore, the proton affinity values of **1**–**4** are subject to uncertainties associated with the entropy change accompanying the protonation process. With regards to this question, it seems that the presently published proton affinities values of **1**–**3** [24] could be slightly overestimated (see the final part of the discussion).

Examination of Table 1 reveals that the dehydration products are always more stable than those corresponding to the ammonia loss. It is generally observed that the dehydration reaction is dominant from low energy protonated aminoethanol, $\mathbf{1H}^+$, and aminopropanol, $\mathbf{2H}^+$, while the reverse stands for protonated aminobutanol, $\mathbf{3H}^+$, and aminopentanol, $\mathbf{4H}^+$. There is consequently no direct relationship between the branching ratio of the two dissociation processes and the stability of the products. The second observation emerging from Table 1 is that protonated cyclic amines and ether are more stable than their protonated imine or aldehyde counterpart only for 5-membered rings or higher. It is, thus, by no means evident that exclusive formation of cyclic ions should be observed from protonated aminoethanol, $\mathbf{1H}^+$, or aminopropanol, $\mathbf{2H}^+$. These two remarks, at least, demonstrate if necessary the interest to correctly assign the product ion structures and to examine in detail the potential energy change associated with the dehydration and deamination reactions of ions $\mathbf{1H}^+$–$\mathbf{4H}^+$ depicted in Scheme 1.

Table 1
Thermochemistry of the deamination and dehydration reactions from protonated aminoalcohols **1**–**4** (heats of formation, in the ion convention, and heats of reaction in kJ mol^{-1})

Species	$\Delta_f H^{\circ}_{298}$	ΔH°_{298}
Protonated aminoethanol $[\mathbf{1H}]^+$	394.5[a]	0
$[Aziridine]H^+ + H_2O$	509.2[c]	114.7
$[Acetaldimine]H^+ + H_2O$	415.2[d]	20.7
$[Oxirane]H^+ + NH_3$	657.3[c]	262.8
$[Acetaldehyde]H^+ + NH_3$	549.8[c]	155.3
Protonated aminopropanol $[\mathbf{2H}]^+$	343.4[a]	0
$[Azetidine]H^+ + H_2O$	443.8[c]	100.4
$[Propanimine]H^+ + H_2O$	394.2[d]	50.8
$[Oxetane]H^+ + NH_3$	602.3[c]	258.9
$[Propanal]H^+ + NH_3$	510.7[c]	167.3
Protonated aminobutanol $[\mathbf{3H}]^+$	310.5[a]	0
$[Pyrrolidine]H^+ + H_2O$	336.2[c]	25.7
$[Butanimine]H^+ + H_2O$	367.2[d]	56.7
$[Tetrahydrofurane]H^+ + NH_3$	477.8[c]	167.3
$[Butanal]H^+ + NH_3$	483.9[c]	173.4
Protonated aminopentanol $[\mathbf{4H}]^+$	282[b]	0
$[Piperidine]H^+ + H_2O$	285.3[c]	3.3
$[Pentanimine]H^+ + H_2O$	342.2[d]	60.2
$[Tetrahydropyrane]H^+ + NH_3$	438.3[c]	156.3
$[Pentanal]H^+ + NH_3$	457.0[c]	175.0

[a] Calculated from G2(MP2) atomization energies, see text.
[b] Estimated from $\Delta_f H^{\circ}_{298}$ $[\mathbf{3H}]^+$ and an extra stabilization situated between the increment of a CH_2 group [22] and the difference in enthalpy between $[\mathbf{2H}]^+$ and $[\mathbf{3H}]^+$.
[c] Using $\Delta_f H^{\circ}_{298}(H_2O) = -241.8$ kJ mol^{-1} and $\Delta_f H^{\circ}(NH_3) = -45.9$ kJ mol^{-1}. The $\Delta_f H^{\circ}_{298}$ of the fragment ions were calculated by combining the heat of formation [21] and the proton affinity [23] of the corresponding neutral with $\Delta_f H^{\circ}_{298}[H]^+ = 1530.0$ kJ mol^{-1}.
[d] From [15a].

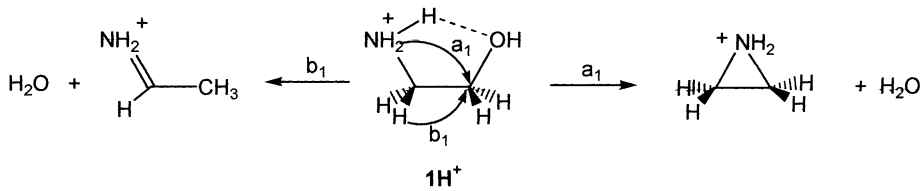

Scheme 2.

3.1. Protonated 1,2-aminoethanol, $1H^+$

Previous studies [5,7–11] have demonstrated that the major fragmentation of protonated aminoethanol, $\mathbf{1H}^+$, is the water loss. Accordingly, the chemical ionization mass spectrum of **1** exhibits a major peak at *m/z* 44 $[\mathbf{1H}–H_2O]^+$. The $[\mathbf{1H}–NH_3]^+$ signal amounts for less than 10% of the peak $[\mathbf{1H}–H_2O]^+$. Under CA of high [8] or low [9,10] energy, $\mathbf{1H}^+$ still eliminates predominantly a water molecule, the competitive ammonia loss representing only 10–30% of the water loss. The dehydration reaction is also responsible of the lone signal observed in the MIKE spectrum of $\mathbf{1H}^+$. When $\mathbf{1_{d3}D}^+$ ($ND_2CH_2CH_2OD + D^+$) ions, produced by deuterium exchanges with D_2O in the ion source, are selected, the signal in the MIKE spectrum corresponds to $[\mathbf{1_{d3}D}–OD_2]^+$. The water loss consequently implies only the hydrogens initially located on the heteroatoms, no exchange with the carbon hydrogens is observed. The shape of the metastable peak associated with the dissociation $\mathbf{1H}^+ \rightarrow [\mathbf{1H}–H_2O]^+$ is a simple Gaussian and its analysis leads to the kinetic energy release values: $T_{0.5} = 32 \pm 3$ meV and $T_{\text{average}} = 95 \pm 9$ meV.

Considering the two possible reaction mechanisms presented in Scheme 1, the dehydration of $\mathbf{1H}^+$ is expected to give either protonated aziridine (path a_1, Scheme 2) or protonated acetaldimine (path b_1, Scheme 2).

Protonated aziridine and protonated acetaldimine are the two most stable $C_2H_6N^+$ ions containing the CCN connectivity and their experimental characterization by CA has been recently reconsidered [15b]. Briefly, it may be recalled that very similar CA spectra are observed for both ions when helium is used as target gas, but that the use of O_2 rather than He induces more differences in the CA mass spectra. The most significant are (i) the presence of a characteristic peak at *m/z* 29, corresponding to a methyl loss, for protonated acetaldimine, and (ii) an intense *m/z* 42 signal for protonated aziridine. Table 2 shows the partial CA (O_2) mass spectra of protonated aziridine, protonated acetaldimine and ions $[\mathbf{1H}–H_2O]^+$ coming from dissociations of $\mathbf{1H}^+$ in the ion source ("S") or in the FFR.

It is noteworthy that the CA mass spectrum of the ions $[\mathbf{1H}–OH_2]^+$ produced in the ion source presents significant peaks at *m/z* 29 and 42 demonstrating the

Table 2
CA/MIKE spectra of $[C_2H_6N]^+$ (*m/z* 44) ions produced by chemical ionization of 1,2-aminoethanol, **1**, and aziridine, and by electron ionization of 1,2-aminopropane, **2APr**, respectively[a]

	43	42	41	40	39	38	30	29	28	27	26	25	18	17	16	15	14	13	12
$[\mathbf{1H}–H_2O]^+$(S)[b]	62	160	62	36	8	5	6	46	100	41	19	2	38	1	<1	15	1	–	–
$[\mathbf{1H}–H_2O]^+$(FFR)[c]	88	305	93	59	20	15	22	14	100	54	25	9	48	–	–	11	–	–	–
$[\mathbf{2Apr}–CH_3]^+$	27	78	34	21	6	3	3	62	100	41	22	4	49	5	1	27	5	<1	–
$[\text{Aziridine}]H^+$	43	128	48	33	11	8	14	20	100	44	23	6	68	5	3	24	6	1	<1

[a] Collision gas: O_2.
[b] Ions formed in the ion source.
[c] Ions produced in the third field-free region of the four sectors mass spectrometer.

presence of protonated acetaldimine and protonated aziridine. Roughly, using the ratio of peak intensities (*m*/*z* 42)/(*m*/*z* 41) and (*m*/*z* 29)/(*m*/*z* 27), the present data may be interpreted by the existence of a mixture of $C_2H_6N^+$ ions containing comparable proportions of both structures. Neutralization–reionization (NR) experiments confirm the formation of a mixture of structures by dehydration of $\mathbf{1H}^+$ in the ion source. Accordingly, the NR mass spectrum of protonated aziridine is characterized by peaks at *m*/*z* 43 and 41 on one hand, and *m*/*z* 28 and 27 on the other, of comparable intensities. For protonated acetaldimine the situation is clearly different since the ratio of peak intensities (*m*/*z* 43)/(*m*/*z* 41) and (*m*/*z* 28)/(*m*/*z* 27) are equal to ca. 1.6. In fact, the NR mass spectrum of ions $[\mathbf{1H}–OH_2]^+$ is intermediate between the two reference spectra (the two preceding ratio of peak intensities are equal to 1.3 and 1.2, respectively) in agreement with the existence of a mixture in equivalent amount of protonated aziridine and protonated acetaldimine.

When considering now the $[\mathbf{1H}–OH_2]^+$ ions produced in the third field-free region of the six sector mass spectrometer, it clearly appears that the CA mass spectrum ("FFR" Table 2) shows a *m*/*z* 29 peak of very low intensity and a (*m*/*z* 42)/(*m*/*z* 41) ratio close to 3.0, as already observed for protonated aziridine. In summary, collisional experiments demonstrate that ions $\mathbf{1H}^+$ of low internal energy lead to protonated aziridine by loss of a water molecule but that a significant amount of protonated acetaldimine is competitively produced from ions of higher internal energy. This reveals a more complicated situation than previously assumed.

The following theoretical part will bring information on the energy required by the two dehydration processes a_1 and b_1 presented in Scheme 2. Concerning the ammonia loss, which represents a minor dissociation route from high internal energy $\mathbf{1H}^+$ ions, only the formation of protonated acetaldehyde (reaction b_2, Scheme 1) has been considered since, as it will be seen below, the set of products $[\text{oxirane}]H^+ + NH_3$ is significantly higher in energy than the transition structures leading to water loss. During the reaction modeling at the MP2/6-31G* level, it has been found that the formation of protonated aziridine involves three successive steps while protonated acetaldimine (or acetaldehyde) is produced via a 1,2-hydrogen migration concerted with a CO (or CN) bond elongation. The various steps of these reaction channels are summarized in Scheme 3 and the corresponding MP2/6-31G* optimized structures are presented in Fig. 1. The corresponding energies are reported in Table 3 and illustrated by the 0 K energy diagram sketched in Fig. 2.

The proton affinity of a primary amine is higher than that of a primary alcohol by ca. 120 kJ mol^{-1} [20]. It is thus, not surprising to find that the nitrogen atom is the preferential protonation site of 1,2-aminoethanol. The most stable conformation of the N-protonated aminoethanol, $\mathbf{1H_a}^+$, presents an internal hydrogen bond characterized by a O···H–N distance of 2.00 Å and a dihedral angle NCCO of 48.1° (Fig. 1). The stabilization energy of this structure may be estimated by a comparison with the *trans* structure $\mathbf{1H_b}^+$. The energy difference (39 kJ mol^{-1} at the MP2(FC)/6-31G* + ZPE level, Table 3) is far from the stabilization energy of the complex $CH_3OH/CH_3NH_3^+$ (93 kJ mol^{-1} at the same level of theory, 80 kJ mol^{-1} from experiment [25]). This weakening of the internal hydrogen bond, which is not unexpected in such a strained system, it is also reflected by the bond length of 2.00 Å, considerably higher than the 1.672 Å calculated for $CH_3OH/CH_3NH_3^+$. It may be noted that conformer $\mathbf{1H_b}^+$, is 129 kJ mol^{-1} lower in energy than the most stable conformation of the O-protonated molecule ($\mathbf{1C_1}$–**N**, Fig. 1, Table 3), in good agreement with the proton affinity difference between a primary amine and a primary alcohol recalled above.

The cyclodehydration reaction of $\mathbf{1H}^+$ starting from structure $\mathbf{1H_a}^+$ (path a_1, Scheme 3) needs the transfer of one proton from the nitrogen atom to the oxygen before the ring closure. Internal proton transfer has been first explored by reducing the $O_1 \cdots H_{11}$ distance (Fig. 1). At the HF/6-31G* level, this process leads to a stable structure, where the proton is located on the oxygen and an internal hydrogen bond is created with the nitrogen, $\mathbf{1H_d}^+$, is found. This structure is situated 115 kJ mol^{-1} above $\mathbf{1H_a}^+$. At the

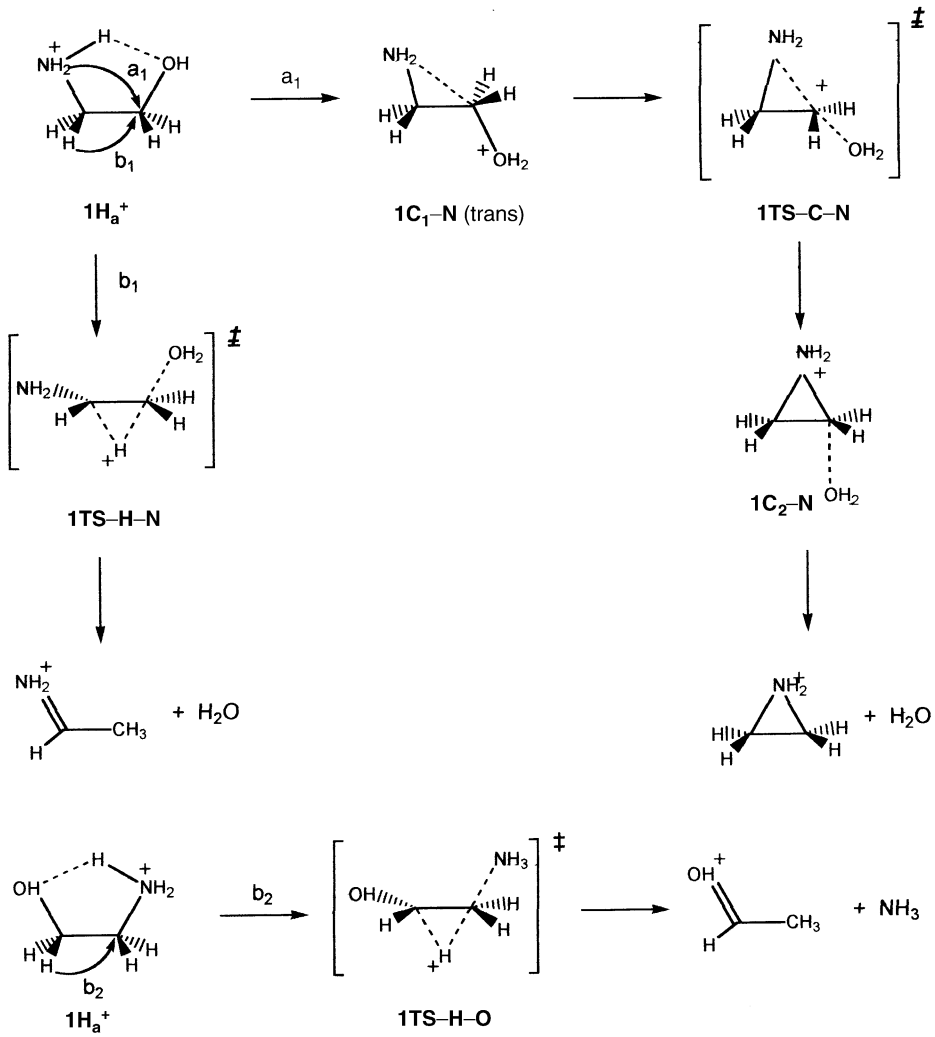

Scheme 3.

MP2(FC)/6-31G* level, however, $\mathbf{1H_d}^+$ collapses to $\mathbf{1H_a}^+$ and it is found that the proton transfer must be coupled with a rotation around the C–N bond in order to attain a *trans* conformation preventing the proton to return back to the nitrogen atom. This stable structure, **1C$_1$–N** (Fig. 1), lies in a shallow potential energy well situated between the two transition structures **1TS–R** and **1TS–C–N**. The transition structure **1TS–R** resembles closely structure **1C$_1$–N** (the essential difference is the NCCO angle value of 130.7° for **1TS–R** and 178.2° for **1C$_1$–N**). **1TS–R** is situated 183 kJ mol^{-1} above $\mathbf{1H_a}^+$ and 15 kJ mol^{-1} above **1C$_1$–N** (MP2/6-31G* + ZPE level, Fig. 2). It may be noted that structure **1C$_1$–N** is partly stabilized by a favorable electrostatic interaction between the carbon atom C$_3$ (Fig. 1), which is bearing a positive charge of 0.49, and the lone pair of the nitrogen atom. This interaction foreshadows the subsequent intramolecular nucleophilic substitution process. The rear attack by the nitrogen toward the carbon C$_3$ induces the elimination of the water molecule through the transition structure **1TS–C–N** characterized by

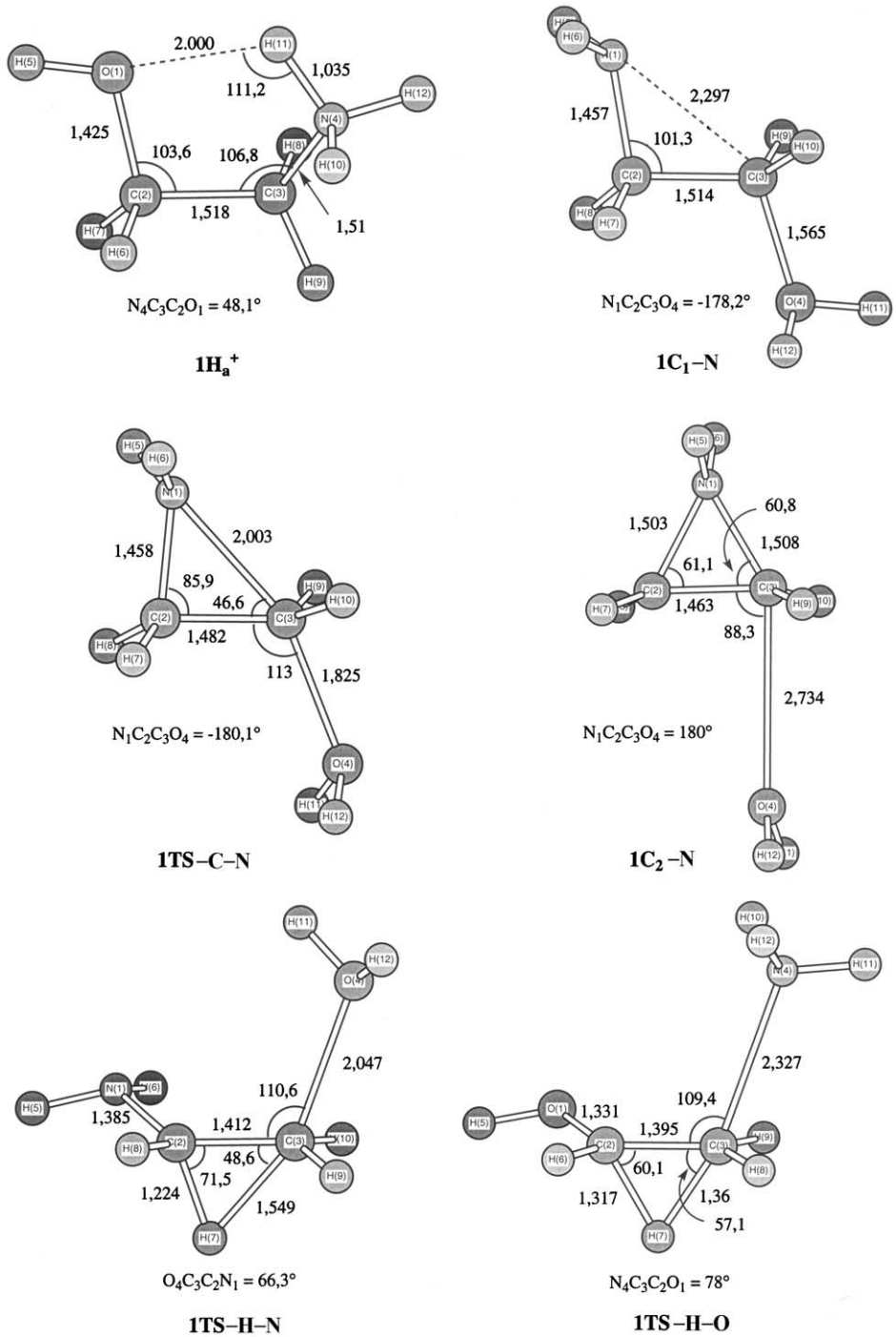

Fig. 1. MP2/6-31G(d) optimized geometry of the species involved during dissociation of protonated 1,2-aminoethanol, **1** (bond lengths in Å, bond angles in °).

Table 3
Calculated total electronic energies (Hartree) and relative energies (kJ mol^{-1}) of the species relevant to the protonated 1,2-aminoethanol, **1H$^+$**, system

Species	HF/6-31G*		MP2(FC)/6-31G*			
	Total	Rel	Total	Rel	ZPE[a]	Rel 0 K
1H$_a$$^+$	−209.47186	0	−210.07355	0	294	0
1H$_b$$^+$	−209.45819	36	−210.05778	41	292	39
1H$_d$$^+$	−209.42800	115	–	–	–	–
1TS–R	−209.40273	182	−210.00084	191	286	183
1C$_1$–N	−209.40828	167	−210.00627	177	285	168
1TS–C–N	−209.40046	187	−210.00002	193	280	179
1C$_2$–N	−209.43459	98	−210.03605	98	280	84
[Aziridine]H$^+$	−133.40795	–	−133.82137	–	220	–
H_2O	−76.01075	–	−76.19685	–	55	–
[Aziridine]H$^+$ + H_2O	−209.41870	140	−210.01822	145	275	126
1TS–H–N	−209.38161	237	−209.97897	248	270	224
[Acetaldimine]H$^+$	−133.44290	–	−133.84898	–	214	–
[Acetaldimine]H$^+$ + H_2O	−209.45365	48	−210.04583	73	269	48
1TS–H–O	−209.38049	240	−209.97982	246	271	223
[Acetaldehyde]H$^+$	−153.22612	–	−153.64486	–	178	–
NH_3	−56.18436	–	−56.35421	–	90	–
[Acetaldehyde]H$^+$ + NH_3	−209.41048	161	−209.99907	195	268	169
[Oxirane]H$^+$	–	–	−153.60459	–	183	
[Oxirane]H$^+$ + NH_3	–	–	−209.95880	301	273	280

[a] Zero-point vibrational energy (MP2/6-31G* corrected by a factor 0.967 [19]), in kJ mol^{-1}.

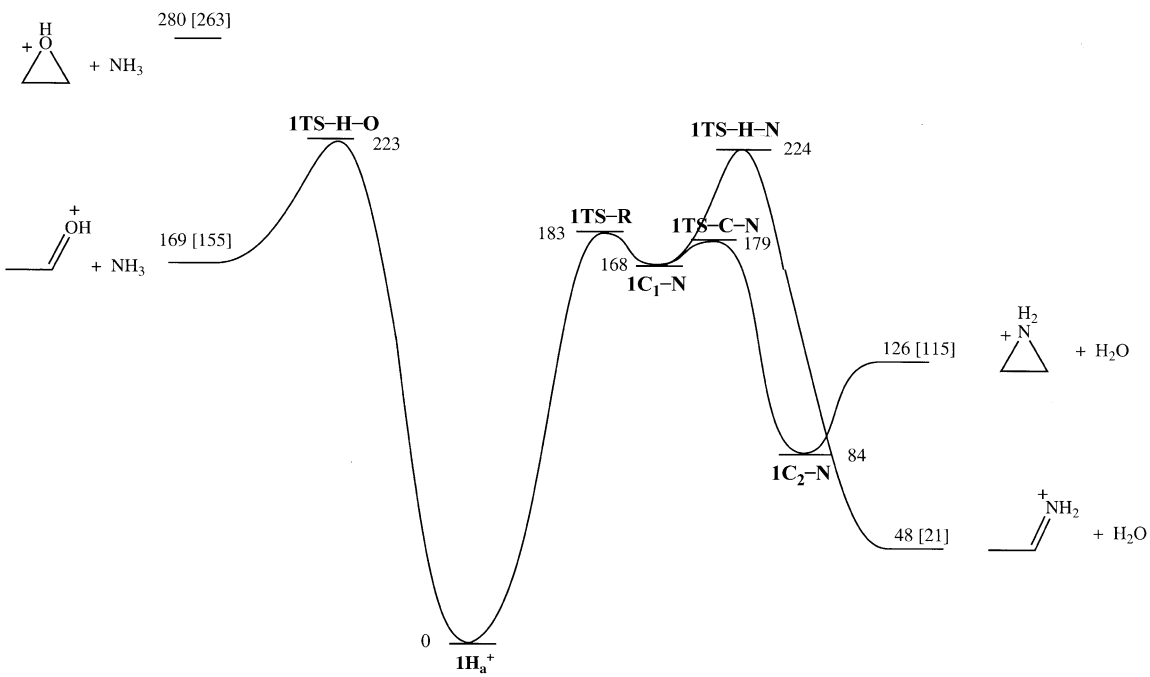

Fig. 2. Calculated 0 K energy profile (kJ mol^{-1}) for the water and ammonia losses from protonated 1,2-aminoethanol. Relative energies calculated at the MP2/6-31G(d) + ZPE level (into brackets are indicated the corresponding 298 K enthalpy variation).

N1–C3 and C3–O4 distances of 2.003 and 1.825 Å, respectively (Fig. 1). The process continues by the lengthening of C3–O4 and the shortening of N1–C3 until attainment of a complex between protonated aziridine and the water molecule, **1C$_2$–N**. This complex, where the C3–O4 distance is extended to 2.734 Å, enjoys a stabilization of 42 kJ mol^{-1} with respect to its components. Its dissociation, into [aziridine]H$^+$ + H$_2$O, is expected to occur without any reverse critical energy. The two transition structures **1TS–R** and **1TS–C–N** are approximately at the same energy level (183 and 179 kJ mol^{-1}, respectively, Fig. 1) and are situated only ∼10 kJ mol^{-1} above the stable conformer **1C$_1$–N** but ca. 50 kJ mol^{-1} above the dehydration products. In outline, it can be said that most of the energetic cost of the cyclodehydration reaction a_1 is the proton transfer from the nitrogen to the oxygen atom in order to form the intermediate structure **1C$_1$–N**.

Obviously, the second dehydration route (b_1, Scheme 3) is also preceded by a proton transfer from the nitrogen to the oxygen. As indicated before, the lone O-protonated structure, predicted to be stable at the MP2/6-31G* level, is the *trans* conformer **1C$_1$–N**. A slight distortion of this structure associated with a 1,2-hydride ion migration open the possibility of water loss through the transition structure **1TS–H–N** (Fig. 1). The overall critical energy of the process **1H$_a$**$^+$ → [acetaldimine]H$^+$ + H$_2$O is equal to 224 kJ mol^{-1} (Fig. 2). It may be considered as resulting from the addition of two energetic contributions: the intramolecular proton transfer giving access to structure **1C$_1$–N** and to the concerted 1,2-H migration/C–O bond elongation. This later contribution renders the reaction path b_1 unfavorable with respect to the cyclodehydration a_1 as clearly evidenced in Fig. 1.

Finally, the deamination process b_2 (Scheme 3) leading to [acetaldehyde]H$^+$ + NH$_3$ has been investigated. The mechanism involves a 1,2-hydride ion migration concerted with a C–N bond elongation. That time, the starting structure **1H$_a$**$^+$ brings the native neutral and thus no proton migration is needed. The transition structure for the reaction, **1TS–H–O**, is calculated to be 223 kJ mol^{-1} above **1H$_a$**$^+$. This energy is considerably higher than that required for the concerted 1,2-H migration/C–O bond elongation, **1C$_1$–N** → [acetaldimine]H$^+$ + H$_2$O (critical energy 56 kJ mol^{-1}), depicted above. As already emphasized, this phenomenon is due to the large difference in dissociation enthalpies of C–XH$^+$ (X = OH, NH$_2$) bonds [15b]. For example, the dissociation enthalpies of CH$_3$–XH$^+$ are 280 and 440 kJ mol^{-1} for X = OH and NH$_2$, respectively, in keeping with the ability of the heteroatoms to share their lone pair electrons.

Note that the second possible deamination reaction (path a_2, Scheme 1) leads to products (protonated oxirane + NH$_3$) situated 280 kJ mol^{-1} above **1H$_a$**$^+$, i.e., 100 kJ mol^{-1} above the transition structures **1TS–R** and **1TS–C–N**, this reaction is consequently excluded.

From the general energy profile given in Fig. 2, it consequently appears that the cyclodehydration reaction a_1 is the most favored dissociative process for **1H**$^+$ ions. The corresponding transition structure is 45 kJ mol^{-1} below the two other: **1TS–H–N** and **1TS–H–O** which corresponds to the dehydration b_1 and to the deamination b_2. The calculations confirm the experimental observation that **1H**$^+$ ions of low internal energy lead exclusively to protonated aziridine. The competitive formation of protonated acetaldimine and protonated acetaldehyde at high internal energy is due to the fact that the three reactions posses similar rate constant values in this energy range. In other words, it means that the three reactions have similar frequency factors, this seems reasonable in view of the mechanisms which, always, involve comparably tight transition structures.

*3.2. Protonated 1,3-aminopropanol, **2H**$^+$*

As previously noted, the main behavior of protonated aminopropanol, **2H**$^+$, of high or low internal energy, is the dehydration process [5,7–11]. Two peaks, **2H**$^+$ (*m*/*z* 76) and [**2H**–H$_2$O]$^+$ (*m*/*z* 58) are observed in the methanol chemical ionization spectrum, the signal associated with [**2H**–NH$_3$]$^+$ ions represents less than 10% of the base peak *m*/*z* 58. The

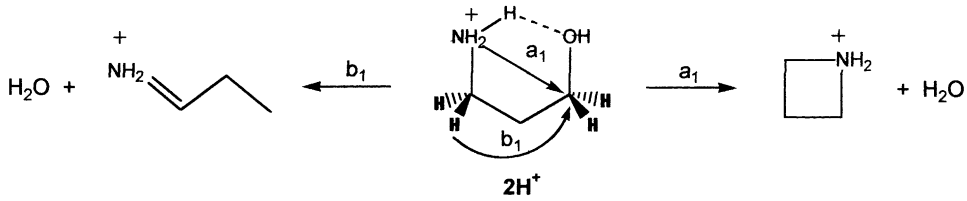

Scheme 4.

MIKE spectrum of $\mathbf{2H}^+$ exhibits only one peak at *m/z* 58 (kinetic energy released: $T_{0.5} = 36 \pm 4$ meV and $T_{\text{average}} = 113 \pm 11$ meV). This peak is fully displaced at *m/z* 60 when the mobile hydrogens of the precursor ion have been exchanged by deuterium in the ion source. The water loss, thus, concerns exclusively the hydrogen atoms borne by the heteroatoms.

From a mechanistic point of view, the two possible dehydration path are the routes a_1 and b_1 depicted in Scheme 4.

Reaction a_1 is an intramolecular nucleophilic substitution giving protonated azetidine while the path b_1 corresponds to a 1,3-hydride ion migration coupled with the water loss to produce protonated propanimine, the most stable $C_3H_8N^+$ ion.

The CA mass spectra of protonated azetidine and protonated propanimine have been compared recently [15b]. The distinction between the two structures is possible through the high intensities of peaks at *m/z* 30 and 57 for the former structure, and at *m/z* 41 for the latter.

Table 4 contains the CA mass spectra of both reference ions and of $[\mathbf{1H}–H_2O]^+$ ions. All in all, the CA mass spectrum of the $[\mathbf{1H}–H_2O]^+$ ions produced in the source matches more closely that of protonated azetidine. However, a noticeable increase of the *m/z* 41 signal and a loss of intensities of *m/z* 30 and 57 point to the presence of a small amount of protonated propanimine. Considering now the CA mass spectrum of the $[\mathbf{1H}–H_2O]^+$ ions produced in the third field-free region of the six sectors mass spectrometer, it appears identical to that of protonated azetidine. Consequently, the loss of H_2O from protonated 1,3-aminopropanol occurs exclusively by intramolecular nucleophilic substitution at low internal energy, whilst the 1,3-hydride shift mechanism becomes weakly competitive at higher energy. This situation, comparable to that encountered for 1,2-aminoethanol,

Table 4
CA/MIKE spectra of $[C_3H_8N]^+$ (*m/z* 58) ions produced by chemical ionization of 1,3-aminopropanol, **2**, and azetidine, and by electron ionization of 2-aminobutane, **2AB**, respectively[a]

		57	56	55	54	52	43	42	41	40	39	38	37	30	29	28	27	26	25	18	15	14
He	$[\mathbf{2H}–H_2O]^+$(S)[b]	11	14	<1	2	<1	17	22	81	9	26	11	6	85	30	100	50	26	4	3	–	–
	$[\mathbf{2AB}–CH_3]^+$	5	17	<1	3	2	34	50	267	15	39	13	7	52	22	100	48	22	2	5	–	–
	[Azetidine]H^+	20	16	1	2	1	14	16	59	9	22	10	5	96	30	100	49	27	–	3	–	–
O_2	$[\mathbf{2H}–H_2O]^+$(S)[b]	23	65	7	13	5	15	21	67	11	25	11	7	78	42	100	39	23	6	1	1	<1
	$[\mathbf{2AB}–CH_3]^+$	8	58	10	15	7	27	40	131	16	33	14	8	43	43	100	37	21	5	2	2	<1
	[Azetidine]H^+	29	70	5	12	4	9	11	55	8	19	9	5	96	36	100	39	23	6	<1	<1	<1
	$[\mathbf{2H}–H_2O]^+$(S)[b]	26	68	6	13	6	15	19	63	11	25	12	7	78	34	100	46	29	9	2	6	4
N_2	$[\mathbf{2H}–H_2O]^+$(FFR)[c]	12	68	5	10	4	8	1	41	8	20	11	6	92	33	100	46	30	10	2	4	3
	$[\mathbf{2AB}–CH_3]^+$	9	52	2	11	5	26	35	124	12	31	11	5	36	24	100	43	23	5	1	6	2
	[Azetidine]H^+	37	62	4	10	3	7	9	38	7	18	9	4	83	32	100	46	29	8	<1	3	2

[a] Collision gas as indicated in the first column.
[b] Ions formed in the ion source.
[c] Ions produced in the third field-free region of the four sectors mass spectrometer.

Table 5
Calculated total electronic energies (Hartree) and relative energies (kJ mol^{-1}) of the species relevant to the protonated 1,3-aminopropanol, **2H**$^+$, system

Species	HF/6-31G*		MP2(FC)/6-31G*			
	Total	Rel	Total	Rel	ZPE[a]	Rel 0 K
2H$_a$ $^+$	−248.51791	0	−249.25228	0	369	0
2H$_b$ $^+$	−248.49787	53	−249.22853	62	367	60
2C$_1$–N	−248.45093	176	−249.18090	187	362	180
2TS–C–N	−248.44195	199	−249.17171	211	358	200
2C$_2$–N	−248.48542	85	−249.21803	90	358	79
[Azetidine]H$^+$	−172.45986	–	−173.00378	–	298	–
H_2O	−76.01075	–	−76.19685	–	55	–
[Azetidine]H$^+$ + H_2O	−248.47061	124	−249.20063	136	353	120
2C$_1$–O	−248.50436	36	−249.23588	43	368	42
2TS–C–O	−248.43828	209	−249.16818	221	356	208
2C$_2$–O	−248.44229	199	−249.17041	215	356	202
[Oxetane]H$^+$	−192.23868	–	−192.79289	–	260	–
NH_3	−56.18436	–	−56.35421	–	90	–
[Oxetane]H$^+$ + NH_3	−248.42304	249	−249.14710	276	350	257
2TS–H–N	−248.41095	281	−249.14494	282	343	256
[Propanimine]H$^+$	−172.48122	–	−173.01845	–	289	–
[Propanimine]H$^+$ + H_2O	−248.49197	68	−249.21530	97	344	72
2TS–H–O	−248.40456	298	−249.13818	300	346	277
[Propanal]H$^+$	−192.26579	–	−192.81538	–	253	–
[Propanal]H$^+$ + NH_3	−250.45015	178	−249.16959	217	343	191

[a] Zero-point vibrational energy (MP2/6-31G* corrected by a factor 0.967 [19]), in kJ mol^{-1}.

1, will be now examined by molecular orbital calculation (Table 5).

The detailed steps of the two dehydration mechanisms a_1 and b_1, as revealed by the calculation, are sketched in Scheme 5.

For a complete understanding of the chemistry of protonated 1,3-aminopropanol, the homologous deamination processes a_2 and b_2 have also been examined, the corresponding steps are presented in Scheme 6.

Optimized geometries of some of the most significant structures are gathered in Fig. 3, the total and relative energies are presented in Table 4 and illustrated by the 0 K energy profile of Fig. 4.

The most stable protonated form of 1,3-aminopropanol is the N-protonated structure **2H$_a$**$^+$ (Fig. 3). This structure is stabilized by an internal hydrogen bond characterized by a NH···O distance of 1.763 Å and a O···H–N angle of 136.9°. The calculated energy difference between **2H$_a$**$^+$ and the full *trans* conformer **2H$_b$**$^+$ is equal to 60 kJ mol^{-1}, demonstrating, as expected, a more efficient hydrogen bonding in protonated 1,3-aminopropanol than in its lower homologue 1,2-aminoethanol. Protonation on the oxygen atom is energetically unfavorable, and, from a structural point of view, stable structure are only possible if the OH_2 group is sufficiently remote from the nitrogen atom to avoid internal proton transfer. We find structure **2C$_1$–N** (Fig. 3) to be the most stable conformer of O-protonated 1,3-aminopropanol, its peculiar stability is due to the existence of an attractive force between the nitrogen atom and the carbon atom **C$_4$** which bears the OH_2 group and consequently a significant positive charge. Structure **2C$_1$–N** plays also a key role in the dehydration mechanisms a_1 and b_1 (Scheme 5). Staring from the global minimum **2H$_a$**$^+$, the formation of **2C$_1$–N** passes through a transition structure corresponding to a dihedral angle **O$_5$**CCC of ∼140° and situated only 4 kJ mol^{-1} above **2C$_1$–N**. The backside nucleophilic attack of **N$_1$** toward **C$_4$**, associated with the C4–O5 bond elongation, leads to an ion/neutral complex **2C$_2$–N** (protonated azetidine/water). The corresponding transition structure **2TS–C–N** (Fig. 3)

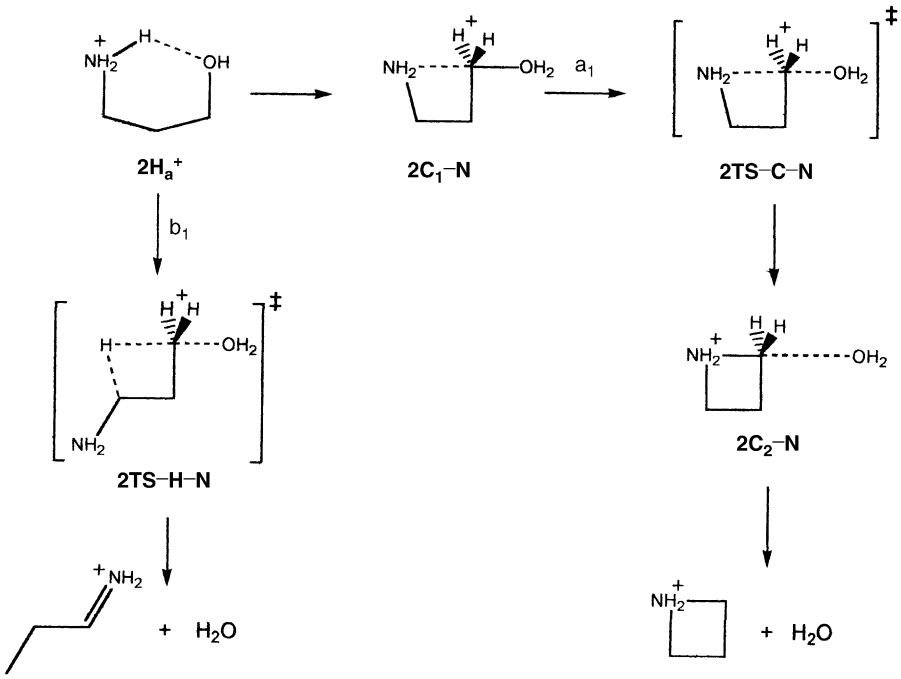

Scheme 5.

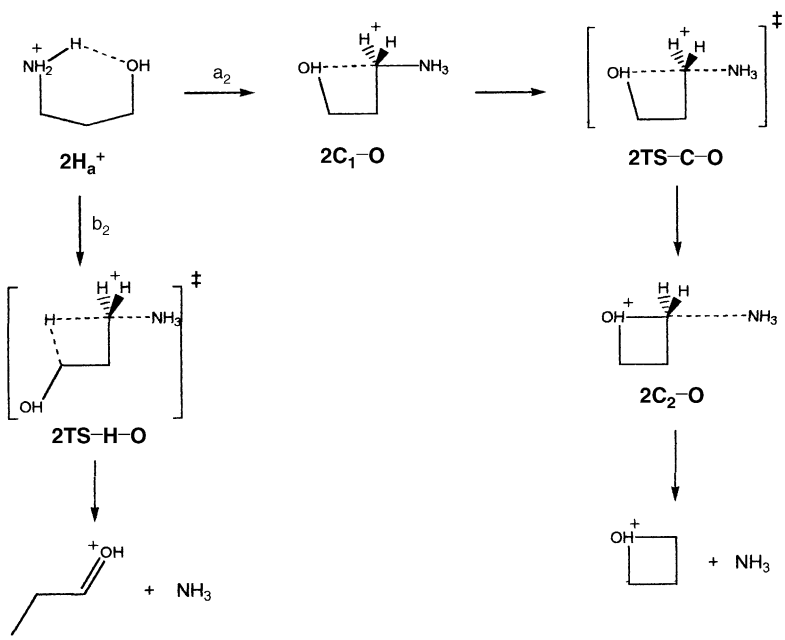

Scheme 6.

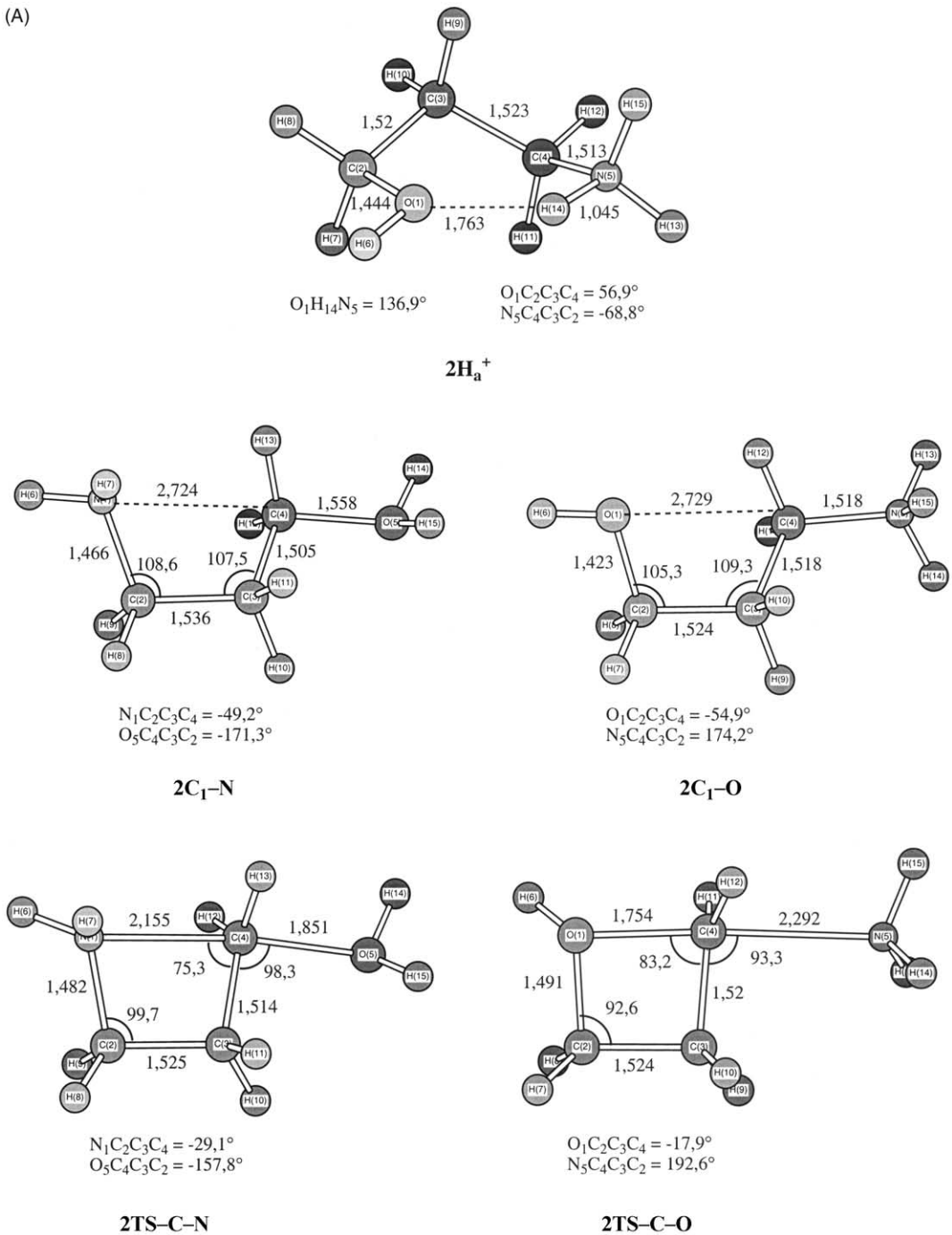

Fig. 3. MP2/6-31G(d) optimized geometry of the species involved during dissociation of protonated 1,3-aminopropanol, **2** (bond lengths in Å, bond angles in °).

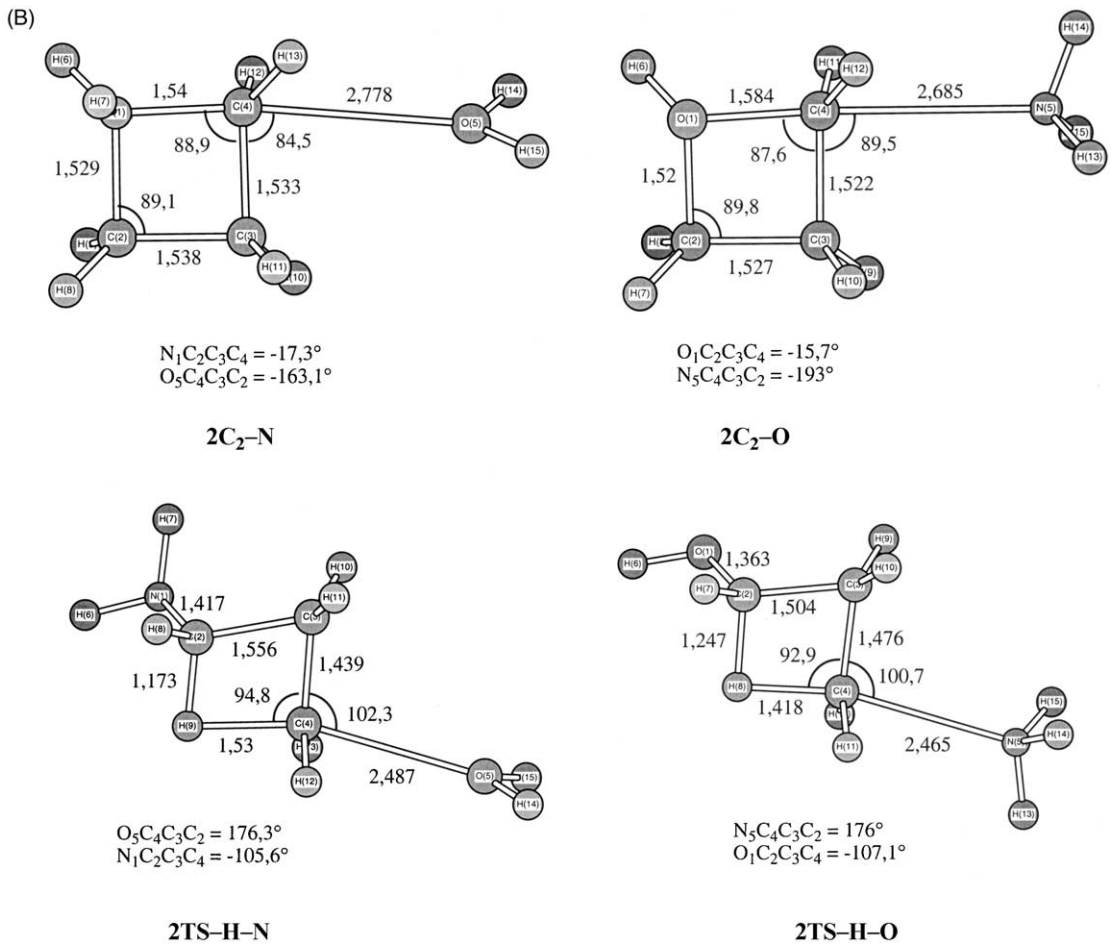

Fig. 3. (*Continued*).

is situated 200 kJ mol^{-1} above $\mathbf{2H_a}^+$. Finally, dissociation of the complex **2C$_2$–N** needs the 41 kJ mol^{-1} of reaction endothermicity, no reverse critical energy is associated with this reaction. In summary, the determinant step of the intramolecular nucleophilic substitution a_1 is the passage through the transition state **2TS–C–N** whose energy of 200 kJ mol^{-1}, is, for the major part, due to the proton transfer from the nitrogen to the oxygen atom.

The second possible dehydration pathway (reaction b_1, Scheme 5) leads to protonated propanimine via a 1,3-hydride ion migration. The starting point of this reaction is easily accounted for by a slight rotation around the C2–C3 bond from **2C$_1$–N** (Scheme 5). This allows the formation of the corresponding transition structure, **2TS–H–N**, which is situated 256 kJ mol^{-1} above $\mathbf{2H_a}^+$ and, consequently, 56 kJ mol^{-1} above the transition structure for reaction a_1, **2TS–C–N** (Fig. 4). No doubt that the latter is the favored dehydration mechanism as attested by the observation of the exclusive formation of protonated azetidine from metastable $\mathbf{2H}^+$ ions.

The loss of a molecule of ammonia represents a minor process from protonated 1,3-aminopropanol. Since the energy of the two possible set of products are below or close to the critical energy for the dehydration reactions, we decided to examine theoretically reactions a_2 and b_2 (Scheme 6). The cyclodeamination

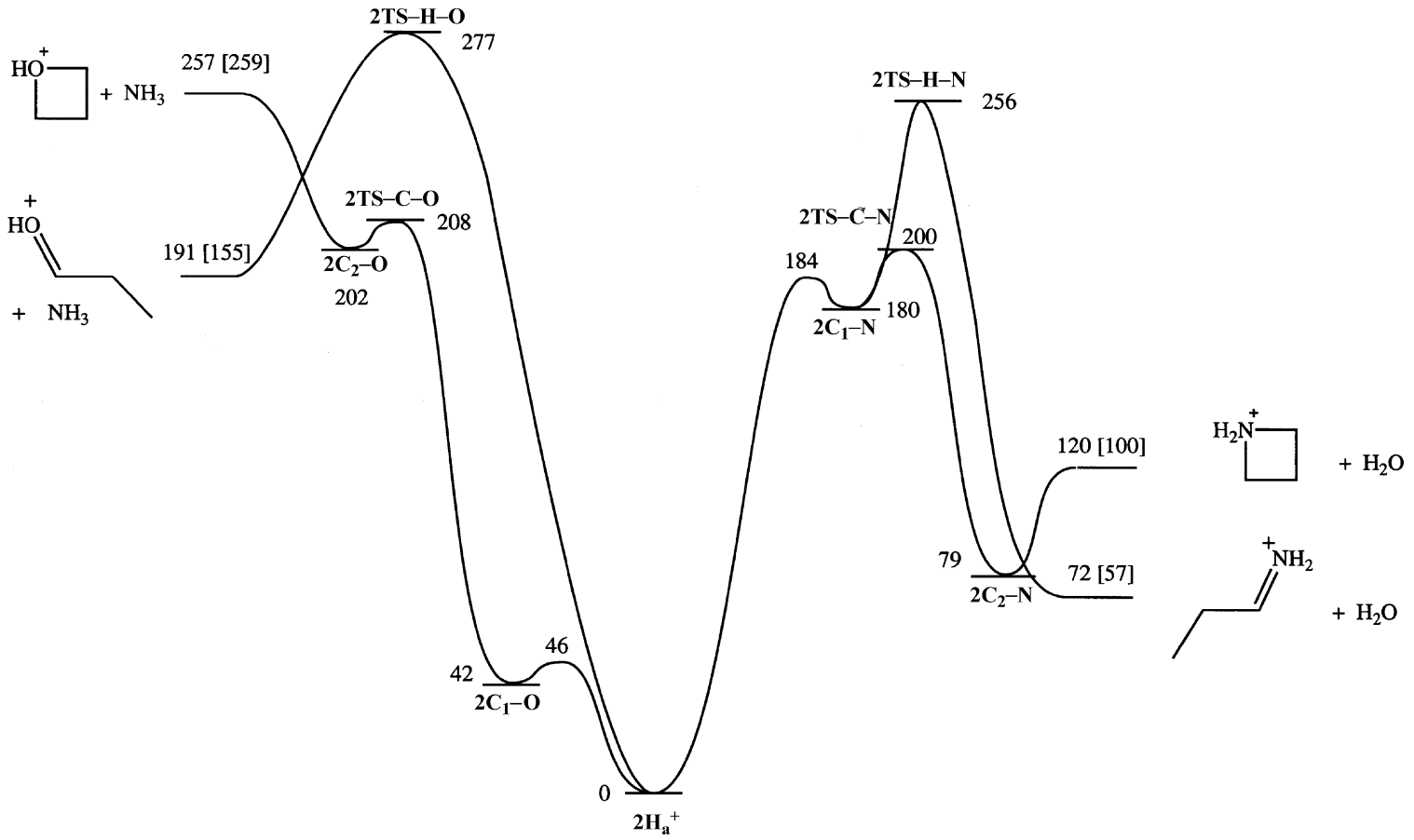

Fig. 4. Calculated 0 K energy profile (kJ mol^{-1}) for the water and ammonia losses from protonated 1,3-aminopropanol. Relative energies calculated at the MP2/6-31G(d)+ZPE level (into brackets are indicated the corresponding 298 K enthalpy variation).

reaction a_2 starts with the formation of the conformer **$2C_1$–O** which is 42 kJ mol^{-1} less stable than **$2H_a^+$**. The passage **$2H_a^+ \rightarrow 2C_1$–O** corresponds to a dihedral angle N_5CCC of 140° and needs only 46 kJ mol^{-1}. The following step is the nucleophilic reaction itself, i.e., the ring closure coupled with the C–N bond elongation. It needs 166 kJ mol^{-1} and leads to a complex between protonated oxetane and ammonia, **$2C_2$–O**. This reaction intermediate dissociates into its components without reverse critical energy. The products, protonated oxetane plus ammonia, being higher in energy than the transition structure **2TS–C–O**, the determining step of the deamination reaction b_1 is simply the separation of the components of the complex **$2C_2$–O**. At this stage, it is tempting to compare the two nucleophilic substitution reactions a_1 and a_2. The most meaningful difference lies in the energy involved by the steps **$2C_1$–N $\rightarrow$ $2C_2$–N** and **$2C_1$–O $\rightarrow$ $2C_2$–O**. The former process is exothermic by 100 kJ mol^{-1} while the latter is endothermic by 160 kJ mol^{-1}. This situation is, again, a reflection of the fact that the dissociation energy of a C–NH_3^+ bond is more than 100 kJ mol^{-1} higher than the dissociation energy of a C–OH_2^+ bond.

Finally, the last reaction, b_2, has been studied. This process leading to protonated propanal by a 1,3-hydride migration concerted with a C–O bond cleavage pass through the transition structure **2TS–H–O** which is situated 277 kJ mol^{-1} above **$2H_a^+$**, it is the process associated with the highest critical energy. Again, this reaction involving a C–O bond cleavage from **$2C_1$–O** is more energy consuming than the reaction b_1 which involves a C–N bond cleavage from **$2C_1$–N**.

In summary, it emerges from the above calculations that the cyclodehydration reaction a_1, giving rise to protonated azetidine, possesses the lowest critical energy. This is in agreement with the exclusive formation of this product ion from **$2H^+$** ions of low internal energy. The parallel formation of protonated propanimine and of [**2H**–NH_3]$^+$ ions, at higher internal energy, may be understood if the rate constants of the competitive processes become comparable at high energy regime. This is in agreement with the calculations which, moreover, suggest that the [**2H**–NH_3]$^+$ ions are presumably protonated oxetane.

3.3. Protonated 1,4-aminobutanol, $3H^+$

The chemical ionization mass spectrum of 1,4-aminobutanol presents peaks at *m/z* 90, 73 and 72 of significant intensities [7–11]. By contrast, dissociation of **$3H^+$** ions of either low or high internal energy in the field-free regions, gives rise, mainly, to *m/z* 73 [8–11]. Accordingly, the MIKE spectrum of **$3H^+$** presents signals at *m/z* 73 [**3H**–NH_3]$^+$ (intensity: 96%) and *m/z* 73 [**3H**–OH_2]$^+$ (intensity: 4%). Comparable results have been reported for collision-induced dissociations in a sector instrument [8] and in a triple–quadrupole apparatus [9]. Deuterium labeling demonstrates that those reactions only involve the hydrogen atoms localized initially on the heteroatoms. The peak associated with the metastable dissociation **$3H^+ \rightarrow$** [**3H**–NH_3]$^+$ is Gaussian in shape and characterized by the kinetic energy release values: $T_{0.5} = 32 \pm 3$ meV and $T_{\text{average}} = 93 \pm 9$ meV.

Scheme 7 presents the four possible pathways of the deamination and dehydration reactions of ions **$3H^+$**.

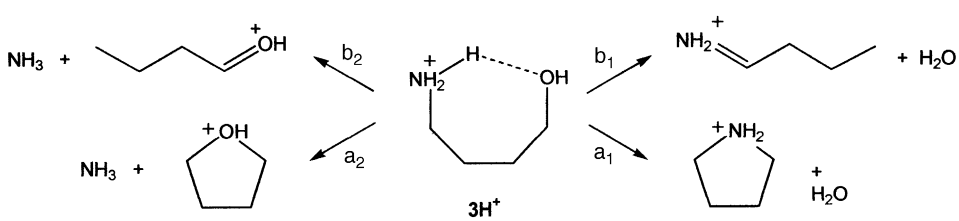

Scheme 7.

The structures of the $C_4H_9O^+$ and $C_4H_{10}N^+$ fragment ions have been identified from their collisional activation mass spectra obtained on the six sectors mass spectrometer. Table 6 contains the CA spectra of the $[\mathbf{3H}–NH_3]^+$ ions produced either in the source or in the third field-free region of the mass spectrometer and the reference $C_4H_9O^+$ ions, i.e., protonated tetrahydrofuran and protonated butanal.

The two reference ions may be identified, whatever the target gas used, by the presence of a peak at *m*/*z* 57 for protonated butanal and *m*/*z* 42 for protonated tetrahydrofuran. Significant differences also appears in the *m*/*z* 27–31 region. It is clear from Table 6 that the CA spectra of $[\mathbf{3H}–NH_3]^+$ ions are identical to that of protonated tetrahydrofuran. Consequently, $C_4H_9O^+$ ions formed by ammonia loss from $[\mathbf{3H}]^+$ precursors of low or high internal energy, are formed by the intramolecular nucleophilic substitution a_2.

Similar investigation has been done for the $C_4H_{10}N^+$ ions, the data are summarized in Table 7. The two reference ions, protonated pyrrolidine and protonated butanimine, may be distinguished particularly by peaks in the *m*/*z* 71–68 and 30–26 regions, and at *m*/*z* 56. The CA mass spectrum of $[\mathbf{3H}–OH_2]^+$ ions produced in the source of the mass spectrometer agrees only with the protonated pyrrolidine structure. Thus, the dehydration reaction also occurs via intramolecular nucleophilic substitution, a_1.

The various reaction intermediates involved during deamination and dehydration of protonated 1,4-aminobutanol $\mathbf{3H}^+$ are summarized in Schemes 8 and 9, respectively. Considering the size of the system, the complete investigation of the corresponding part of the potential energy surface has been done at the HF/6-31G* level, the most important optimized structures are presented in Fig. 5. The energies have been then evaluated at the MP2/6-31G*//HF/6-31G* + ZPE level (Table 8). These data were used to construct the 0 K energy diagram presented in Fig. 6.

The most stable structure of protonated 1,4-aminobutanol is the pseudo-chair N-protonated structure $\mathbf{3H_a}^+$ (Fig. 5). As expected, the internal hydrogen bond is shorter in $\mathbf{3H_a}^+$ than in the lower homologues (1.736 Å for $\mathbf{3H_a}^+$ but 1.879 Å for $\mathbf{2H_a}^+$ and 2.13 Å for $\mathbf{2H_a}^+$, HF/6-31G* optimized geometries). In the same vein, the N–H···O bond angle is larger for $\mathbf{3H_a}^+$ (155° compared to 133° and 106° for $\mathbf{2H_a}^+$ and $\mathbf{1H_a}^+$, respectively). As a consequence, the stabilization energy of $\mathbf{3H_a}^+$ is also larger, an estimate of 67 kJ mol^{-1} is given by the energy difference between $\mathbf{3H_a}^+$ and the linear conformer $\mathbf{3H_b}^+$ (Table 7).

The cyclodeamination reaction a_2 begins with the conformational change $\mathbf{3H_a}^+ \rightarrow \mathbf{3C_1–O}$. During this process, the internal hydrogen bond is broken and replaced by an electrostatic attraction between the carbon atom C_1 and the oxygen. Conformer $\mathbf{3C_1–O}$ is 42 kJ mol^{-1} above the global minimum $\mathbf{3H_a}^+$ from which it is separated by a very small rotational barrier of 2 kJ mol^{-1} (Fig. 6). The ring closure is accompanied by the C–N bond elongation, this step is associated with transition structure **3TS–C–O** situated 166 kJ mol^{-1} above $\mathbf{3H_a}^+$. Further, the system evolves toward the ion/neutral complex $\mathbf{3C_2–O}$ which may dissociate by a simple separation of its components. All the transition structures identified during the overall cyclodeamination process are situated below the energy level of the dissociation products. It consequently appears that the energy determining step is the formation of protonated tetrahydrofuran plus a molecule of ammonia by the simple stretching of the weak C···N bond present in the complex $\mathbf{3C_2–O}$.

The second possible mechanism of ammonia loss (b_2 Scheme 8) possesses a transition structure of too high energy to favorably compete with the previously examined mechanism a_1. Accordingly, structure **3TS–H–O** is situated 284 kJ mol^{-1} above $\mathbf{3H_a}^+$ and 85 kJ mol^{-1} above the products: protonated butanal + NH_3. This result explain why only the protonated tetrahydrofuran is produced from $\mathbf{3H}^+$ ions of low and of high internal energy.

The first step of the cyclodehydration reaction a_1 (Scheme 9) is the proton transfer from the nitrogen to the oxygen atom: $\mathbf{3H_a}^+ \rightarrow \mathbf{3C_1–N}$. The latter structure, which is situated 174 kJ mol^{-1} above $\mathbf{3H_a}^+$, is the most stable O-protonated form of the 1,4-aminobutanol. Starting from $\mathbf{3C_1–N}$, the ring closure along the C–N bond is accompanied by a C–O bond stretching until attainment of the $\mathbf{3C_2–N}$

Table 6
CA/MIKE spectra of $[C_4H_9O]^+$ (*m/z* 73) ions produced by chemical ionization of 1,4-aminobutanol, **3**, butanal and tetrahydrofuran, **THF**, respectively[a]

		72	71	57	55	53	51	50	45	44	43	42	41	40	39	38	37	31	30	29	28	27	26
He	[**3H**–NH_3]$^+$(S)[b]	2	2	4	440	2	2	2	9	32	100	37	25	7	32	7	4	67	19	25	15	41	11
	[Butanal]H^+	8	2	15	251	2	1	1	6	44	100	10	25	4	30	4	1	39	2	54	9	66	10
	THFH$^+$	12	6	3	166	<1	<1	1	8	42	100	44	28	8	32	8	2	60		22	12	37	11
O_2	[**3H**–NH_3]$^+$(S)[b]	9	7	3	518	6	1	1	6	51	100	58	33	9	34	7	4	45	7	18	7	21	7
	But	10	2	60	400	8	3	3	6	93	100	21	33	9	38	12	7	32	6	52	15	47	16
	THF	10	9	4	383	5	3	3	6	58	100	65	38	12	42	12	7	50	5	23	10	29	11
N_2	[**3H**–NH_3]$^+$(S)[b]	10	11	8	419	5	3	3	5	52	100	57	37	13	46	16	10	57	11	32	17	46	24
	[**3H**–NH_3]$^+$(FFR)[c]	14	14	6	338	5	4	4	8	65	100	66	41		51		10	61		35	16	51	25

[a] Collision gas as indicated in the first column.
[b] Ions formed in the ion source.
[c] Ions produced in the third field-free region of the four sectors mass spectrometer.

Table 7
CA/MIKE spectra of $[C_4H_{10}N]^+$ (*m/z* 72) ions produced by chemical ionization of 1,4-aminobutanol, **3**, and pyrrolidine, and by electron ionization of 2-aminopentane, **2APe**, respectively[a]

		71	70	69	68	56	55	54	53	52	51	50	44	43	42	41	40	39	38	37	30	29	28	27	26	15
N_2	$[\mathbf{3H}–OH_2]^+$(S)	13	22	7	18	4	29	7	6	3	4	4	12	100	51	60	22	54	24	13	232	25	100	66	36	4
	$[\mathbf{2APe}–CH_3]^+$	6	10	4	2	67	38	17	6	6	5	4	18	100	72	58	23	53	22	10	176	46	128	90	35	4
	$[Pyrrolidine]H^+$	42	29	6	18	<1	6	2	2	<1	1	1	4	100	40	53	17	43	18	9	147	18	90	53	30	1

[a] Collision gas as indicated in the first column.

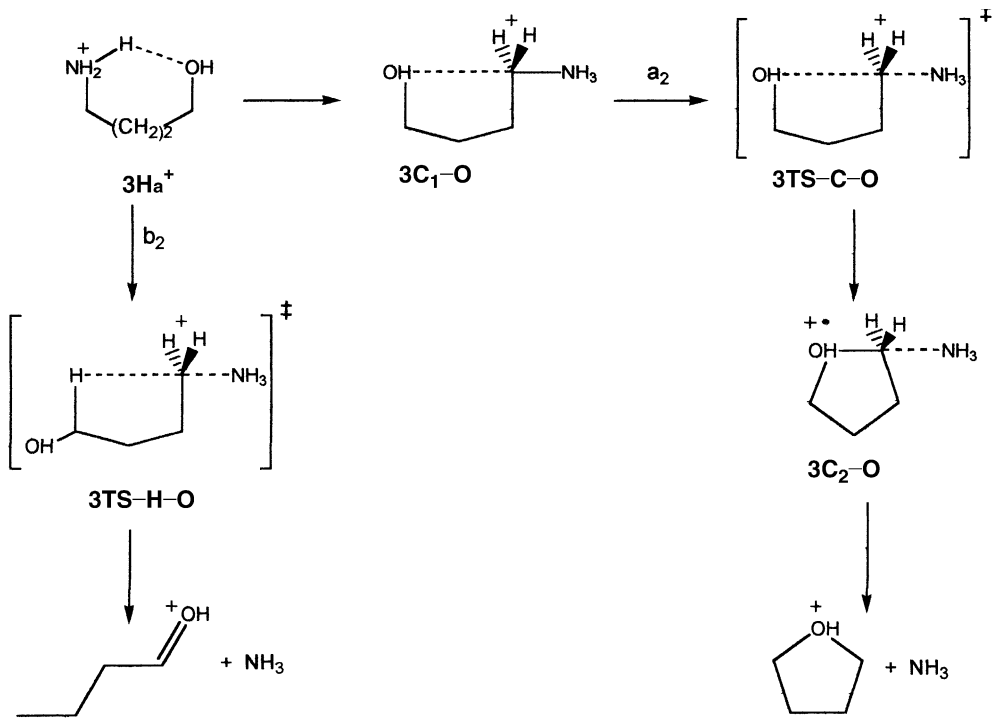

Scheme 8.

ion/neutral complex. As illustrated by Fig. 6, structure **3C$_1$–N** lies in a very shallow potential energy well since it is separated from **3H$_a$**$^+$ by a rotational barrier of 10 kJ mol^{-1} and from **3C$_2$–N** by a barrier of 3 kJ mol^{-1}. Finally, the last step of the reaction is the dissociation of complex **3C$_2$–N** by separation of its components, protonated pyrrolidine and a water molecule. At the level of theory used here, it is hard to decide which of the two steps **3H$_a$**$^+$ → **3C$_1$–N** or **3C$_1$–N** → **3C$_2$–N** is energy determining. However, there is no doubt that most of the energy requirement is the formation of conformer **3C$_1$–N**, i.e., the energy needed by the intramolecular proton transfer from the nitrogen to the oxygen atoms.

This energy is also required by the second dehydration reaction (b_1, Scheme 9). The transition structure of this reaction is 293 kJ mol^{-1} above **3H$_a$**$^+$, the reaction is consequently not competitive with reaction a_1 in agreement with the exclusive formation of protonated pyrrolidine from **3H**$^+$.

In conclusion, the experimental behavior of protonated 1,4-aminobutanol, **3H**$^+$, is easily explained by the two low energy processes a_2 and a_1. Both reactions are intramolecular nucleophilic substitutions leading to cyclized ionic products. Calculation indicates comparable critical energy for the ammonia loss and the water loss (Fig. 6, Table 8). Experimental results suggest that the former reaction possesses a slightly lower critical energy in order to account for the greater intensity of peak *m/z* 73 in the MIKE spectrum of **3H**$^+$.

*3.4. Protonated 1,5-aminopentanol, **3H**$^+$*

Finally, only the experimental results concerning protonated 1,5-aminopentanol, **4H**$^+$ will be reported. The size of the system as well as the obvious conclusions which can be drawn from the three lowest homologues renders unnecessary a theoretical investigation of this molecule.

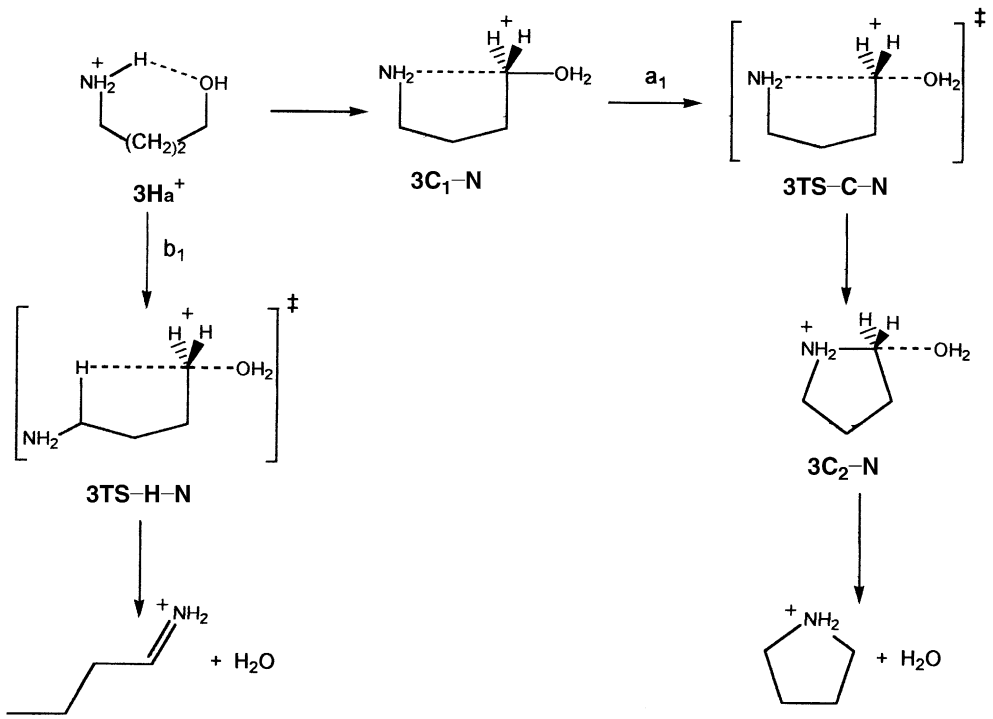

Scheme 9.

The behavior of $\mathbf{4H}^+$ is comparable to that of $\mathbf{3H}^+$, its MIKE spectrum presents three peaks at *m/z* 87 $[\mathbf{4H}–NH_3]^+$ (82%), *m/z* 86 $[\mathbf{4H}–OH_2]^+$ (11%), and *m/z* 69 $[\mathbf{4H}–NH_3–OH_2]^+$ (7%). The main peak is Gaussian and characterized by the kinetic energy releases: $T_{0.5} = 40 \pm 4$ meV and $T_{\text{average}} = 104 \pm 10$ meV.

The four possible reaction pathways for losses of water and ammonia are summarized in Scheme 10.

Product ion structures have been examined, as usual, by CA. The results are gathered in Tables 9 and 10.

The two possible deamination products, protonated tetrahydropyran and protonated pentanal, may be distinguished by comparison of the *m/z* 27–31, 42–45, 53–57 and 67–69 peaks in their CA spectra. We can see, from examination of Table 9, that the CA mass spectra of the $[\mathbf{4H}–NH_3]^+$ ions formed in both the source or the field-free region of the mass

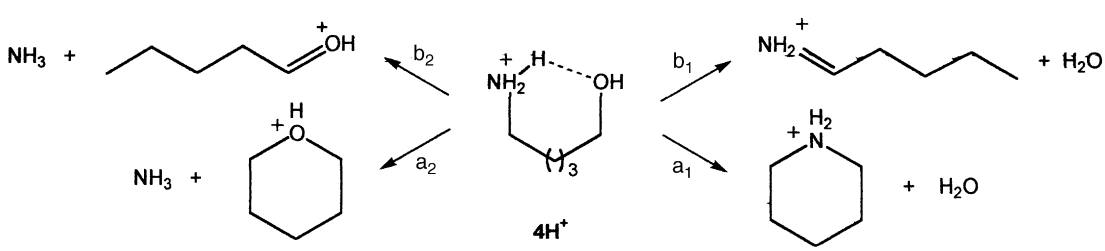

Scheme 10.

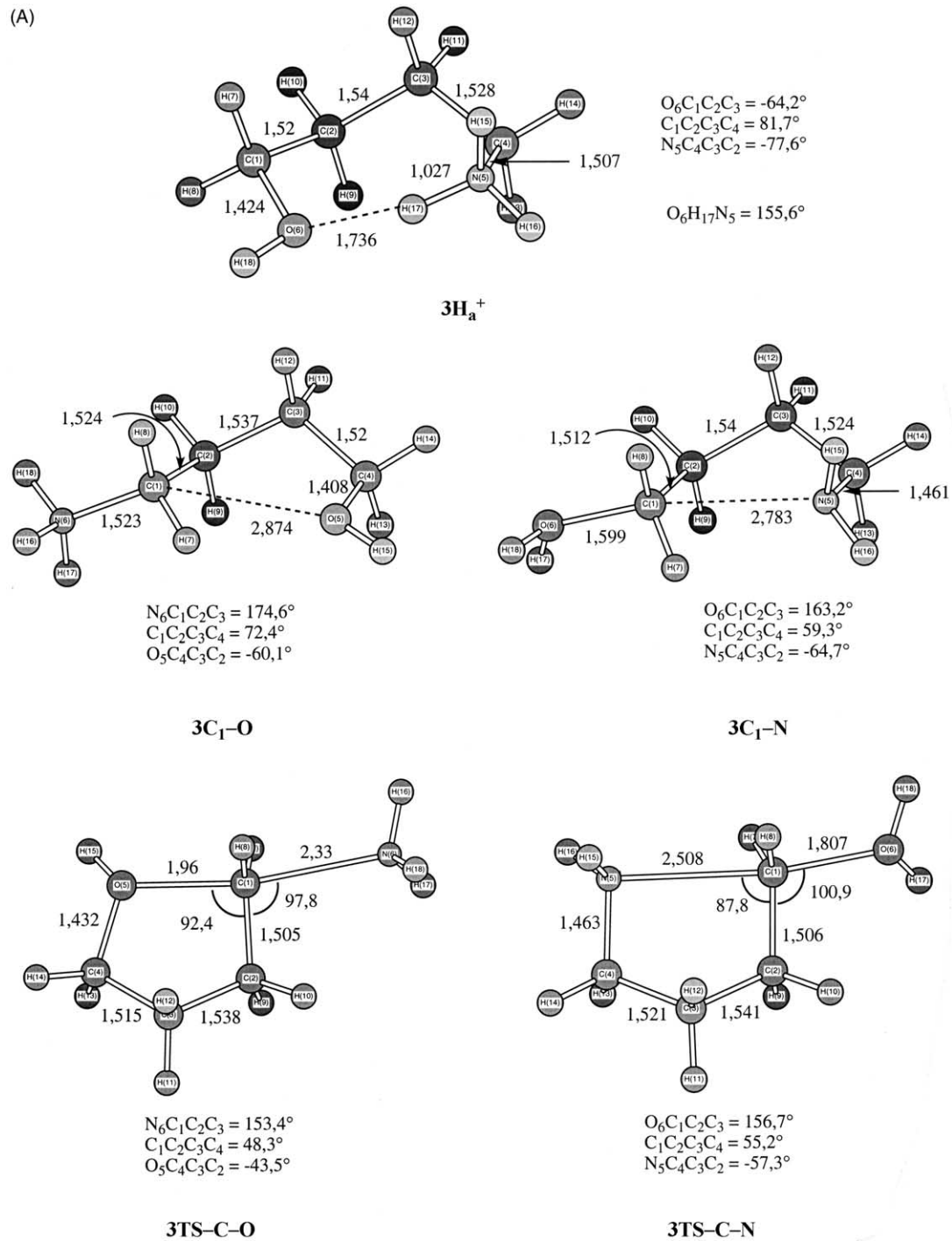

Fig. 5. MP2/6-31G(d) optimized geometry of the species involved during dissociation of protonated 1,4-aminobutanol, **3** (bond lengths in Å, bond angles in °).

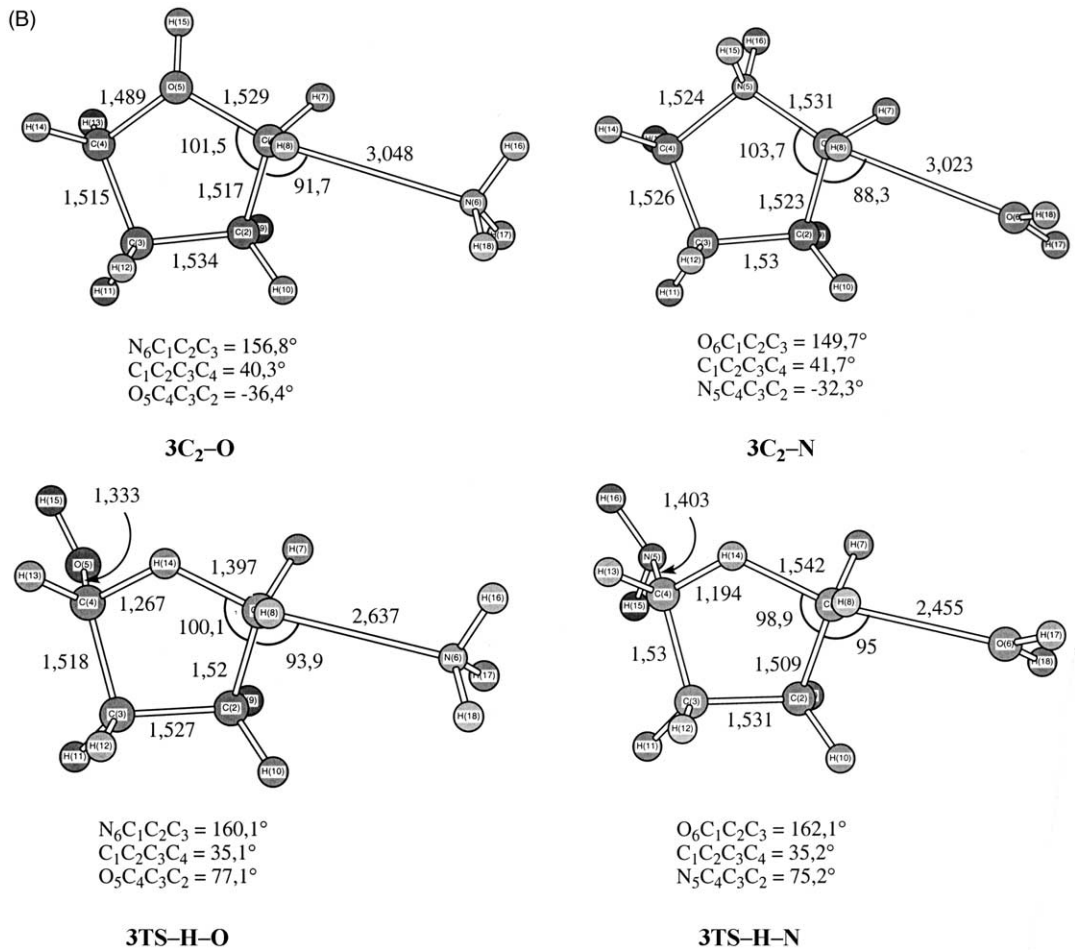

Fig. 5. (*Continued*).

spectrometer, perfectly match that of the protonated tetrahydropyran. The most favored pathway is consequently the intramolecular nucleophilic substitution reaction a_2 (Scheme 10).

The dehydration reaction is expected to give rise to either protonated piperidine or protonated pentanimine. These two structures are easily characterized from their CA mass spectra, particularly in the *m*/*z* 39–44 region. It may be concluded from Table 10 that $[\mathbf{4H}–OH_2]^+$ ions are essentially protonated piperidine and, consequently, that the dehydration reaction occurs exclusively by the internal nucleophilic substitution reaction a_1 (Scheme 10).

These experimental results are in complete analogy with those obtained for the lower homologue $\mathbf{3H}^+$. This has to be expected because a comparable potential energy profile is probably associated to $\mathbf{3H}^+$ and $\mathbf{4H}^+$. Moreover, the formation of the cyclic ionized fragments is even more favored in the latter case by the decrease of the reaction enthalpy (Table 1).

3.5. Protonation thermochemistry

Gas-phase basicity of aminoalcohols **1**–**3** has been determined by Mautner et al. [24] from measurement of proton transfer equilibrium constants in a mass

Table 8
Calculated total electronic energies (Hartree) and relative energies (kJ mol^{-1}) of the species relevant to the protonated 1,4-aminobutanol, **3H**$^+$, system

Species	HF/6-31G*		MP2(FC)/6-31G*//HF/6-31G*			
	Total	Rel	ZPE[a]	Total	Rel	Rel 0 K
3H$_a$ $^+$	−287.55619	0	441	−288.42030	0	0
3H$_b$ $^+$	−287.53448	57	438	−288.39355	70	67
3H$_c$ $^+$	−287.47975	201	431	−288.33708	218	208
3C$_1$–O	−287.54306	34	440	−288.40390	43	42
3TS–C–O	−287.49598	158	427	−288.35194	180	166
3C$_2$–O	−287.50859	125	429	−288.36491	145	133
THFH$^+$	−231.30799	–	335	−231.99216		
NH_3	−56.18436	–	89	−56.35371		
THFH$^+$ + NH_3	−287.49235	168	424	−288.34587	195	178
3C$_1$–N	−287.49079	172	432	−288.35055	183	174
3TS–C–N	−287.48923	176	429	−288.34825	189	177
3C$_2$–N	−287.55325	8	433	−288.41666	10	2
[Pyrrolidine]H$^+$	−211.52894	–	373	−212.20494	–	–
H_2O	−76.01075	–	55	−76.19596	–	–
[Pyrrolidine]H$^+$ + H_2O	−287.53969	43	428	−288.40090	51	38
3TS–H–O	−287.44134	302	415	−288.30235	310	284
[Butanal]H$^+$	−231.30223		324	−231.98026	–	–
[Butanal]H$^+$ + NH_3	−287.48659	183	413	−288.33397	227	199
3TS–H–N	−287.44077	303	413	−288.29793	321	293
[Butanimine]H$^+$	−211.51755	–	360	−212.18399	–	–
[Butanimine]H$^+$ + H_2O	−287.52830	73	415	−288.37995	106	80

[a] Zero-point vibrational energy (HF/6-31G* corrected by a factor 0.913 [19]), in kJ mol^{-1}.

spectrometer equipped with a high pressure ion source. Variable temperature studies allowed also the authors to estimate the ΔH° and ΔS° of the reactions and consequently the proton affinities (PAs) and protonation entropy of the aminoalcohols **1**–**3**. It was found that the gas-phase basicities and proton affinities of the molecules **1**–**3** are enhanced with respect to the corresponding primary amines and that the protonation is accompanied by a significant entropy loss. These observations are in agreement with the formation of a strong internal hydrogen bond in the protonated forms, as already demonstrated by the molecular orbital calculations presented above. In order to fully quantify these effects, we have decided to estimate the thermochemical quantities associated with the protonation process by means of molecular orbital calculations. The following lines will present results of entropy estimations taking into account the rotational barriers of the torsional modes, and proton affinities calculations conducted at the G2(MP2) level.

The method of calculation of absolute third law entropies adopted here uses standard statistical thermodynamic formulae through a procedure comparable to the E_2 method described by Radom and co-workers [26]. Entropies for internal rotations were computed by using the hindered rotor model developed by Pitzer and Gwinn [27]. In this approach, the energy levels of a rotor associated with a potential energy barrier of the form $V_0/2\ (1 - \cos n\phi)$, where ϕ is the dihedral angle, are found with the help of a one-dimensional Schrödinger equation. In practice, the entropy of a given rotor is obtained by subtraction of a corrective term to the entropy calculated under the free rotor approximation, S°_{fr}:

$$S^\circ_{fr} = \frac{1}{2} R \ln \left[\frac{8\pi^3 e I_{red} kT}{n^2 h^2} \right]$$

where $e = 2.71828$ and I_{red} the reduced moment of inertia of the two rotating groups around the axis containing the twisting bond. The corrective term values

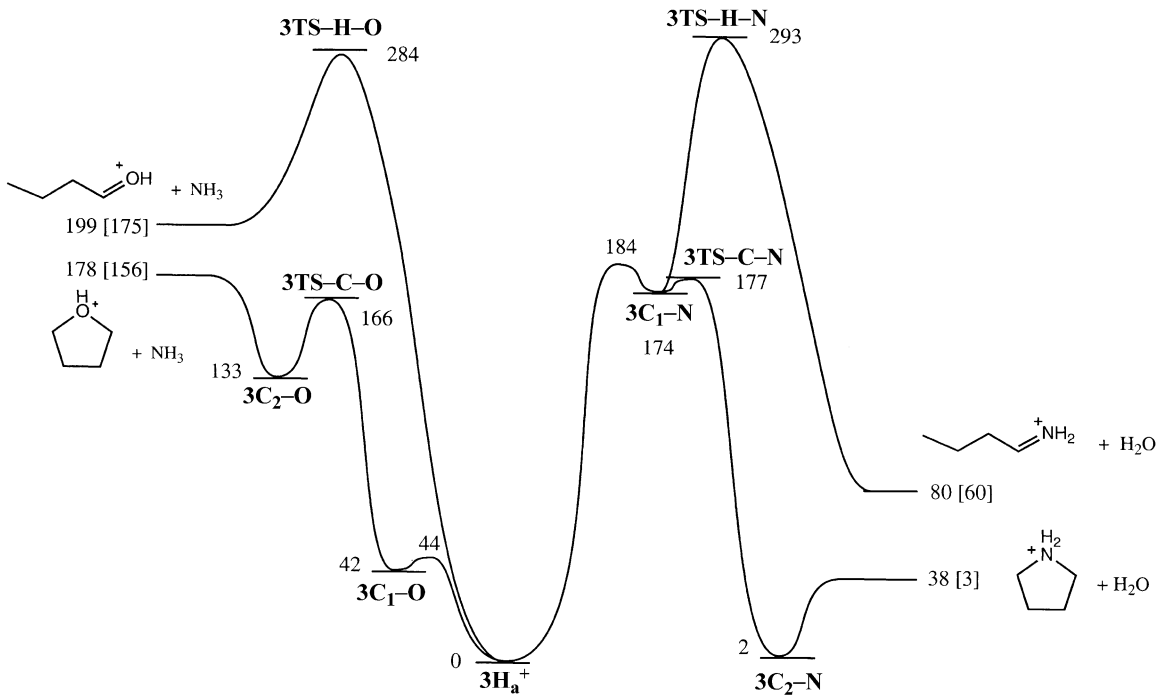

Fig. 6. Calculated 0 K energy profile (kJ mol^{-1}) for the water and ammonia losses from protonated 1,4-aminobutanol. Relative energies calculated at the MP2/6-31G(d) + ZPE level (into brackets are indicated the corresponding 298 K enthalpy variation).

are presented as a function of two dimensionless variables: V_0/RT and $1/Q_{fr}$ (i.e., the reciprocal of the partition function for the free rotation). In the present study, the required rotational potential energy barriers, V_0, were obtained at the HF/6-31G(d) level using a relaxed rotation approach (i.e., all geometrical parameters were optimized except the dihedral angle considered). For the purpose of comparison, the entropy of the corresponding harmonic oscillator was also calculated using the vibrational frequencies of the torsional modes given by the relationship:

$$\nu = \left(\frac{n}{2\pi}\right)\left(\frac{v_0}{I_{red}}\right)^{1/2}.$$

The results obtained for aminoalcohols **1**–**3** and their protonated forms are gathered in Table 11.

Several comments concerning the conformational analysis of the various structures can briefly be made. The MP2/6-31G(d) optimized structures of the neutral molecules **1**–**3** are presented in Fig. 7.

The global minimum on the potential energy surface associated with molecule **1** along the three torsional modes is the conformer g‘Gg’ which presents an internal hydrogen bond between the hydrogen of the hydroxyl group and the lone pair of the nitrogen atom (Fig. 7). Our conformational analysis, thus, confirms the previous findings obtained at lower levels of theory [28]. Note that the *trans* conformer, g‘Tg’, in which the internal hydrogen bond is broken, is situated 12.5 kJ mol^{-1} above conformer g‘Gg’. As shown in Table 11, the rotational barriers along the three axis are of comparable magnitude, the comparison between these energy barriers of ca. 29 kJ mol^{-1} and the difference in energy between **1**g‘Gg’ and **1**g‘Tg’ reveals that a large part of the torsional critical energy is brought by repulsive interactions between eclipsed substituents and not only by the breaking of the internal hydrogen bond. In the protonated form $\mathbf{1H}^+$, rotational barriers around the O1–C2 and the C2–C3 bonds are as high as 69 and 44 kJ mol^{-1}, respectively. The

Table 9
CA/MIKE spectra of $[C_5H_{11}O]^+$ (*m/z* 87) ions produced by chemical ionization of 1,5-aminopentanol, **4**, pentanal and tetrahydropyran, **THP**, respectively[a]

		86	85	71	70	69	68	67	58	57	56	55	54	53	45	44	43	42	41	39	31	30	29	28	27
He	[**4H**–NH_3]$^+$(S)[b]	3	2	–	11	383	14	6	4	39	9	11	4	6	17	11	21	14	100	43	41	13	29	17	30
	[Pentanal]H^+	3	–	–	–	271	–	–	5	91	–	6	–	2	15	34	52	11	100	44	17	1	53	6	50
	THPH$^+$	6	<1	–	–	176	6	<1	<1	48	5	10	1	2	7	4	13	5	100	38	38		24	9	26
	[**4H**–NH_3]$^+$(S)[b]	17	5	3	–	926	41	27	4	60	17	21	11	13	24	19	21	16	100	39	27	8	25	13	19
O_2	[Pentanal]H^+	8	–	4	–	640	–	7	24	145	–	18	8	9	27	95	69	35	100	58	20	9	55	19	40
	THPH$^+$	12	6	3	–	568	44	22	6	56	18	23	12	14	23	20	22	19	100	45	30		30	18	25
N_2	[**4H**–NH_3]$^+$(S)[b]	13	12	10	16	677	36	18	4	60	16	21	9	13	21	18	25	16	100	58	42	14	44	30	53
	[**4H**–NH_3]$^+$(FFR)[c]	8	8	8	9	733	34	16	4	55	11	19	7	11	15	14	19	11	100	56	38	6	41	23	52

[a] Collision gas as indicated in the first column.
[b] Ions formed in the ion source.
[c] Ions produced in the third field-free region of the four sectors mass spectrometer.

Table 10
CA/MIKE spectra of $[C_5H_{12}N]^+$ (*m*/*z* 86) ions produced by chemical ionization of 1,5-aminopentanol, **4**, and piperidine, and by electron ionization of 3-aminoheptane, **3AH**, respectively[a]

		85	84	82	80	70	69	68	67	65	56	54	53	52	51	50	44	43	42	41	39	30	29	28	27
He	$[\mathbf{4H}–OH_2]^+$(S)	12	2	–	–	–	79	15	5	<1	45	6	8	–	3	2	19	31	31	100	55	210	31	45	37
	$[\mathbf{3AH}–C_2H_5]^+$	3	1	<1	–	5	83	3	4	1	113	15	8	5	5	3	45	115	65	100	58	220	40	68	50
	$[Piperidine]H^+$	56	23	3	<1	3	49	8	6	<1	150	21	15	6	7	5	21	50	54	100	64	220	39	60	35
O_2	$[\mathbf{4H}–OH_2]^+$(S)	33	13	4	2	–	202	28	20	4	77	14	14	6	10	7	23	42	32	100	56	205	20	35	22
	$[\mathbf{3AH}–C_2H_5]^+$	4	5	5	6	9	111	10	11	4	187	26	11	9	11	9	45	153	77	100	60	162	40	74	45
	$[Piperidine]H^+$	172	81	19	7	14	88	28	17	1	244	39	21	11	13	10	24	83	67	100	69	239	40	75	39

[a] Collision gas as indicated in the first column.

Table 11
Entropy calculation for the neutral and protonated aminoalcohols **1**–**3**

Species	Bond	V_0[a]	S°[b]	S_t° (free rotation)[c]	S_t° (Pitzer)[c]	S_t° (harmonic oscillator)[c]
1	O1–C2	28.6	312.1	18.9	8.9	6.0
	C2–C3	29.0		31.2	20.8	16.0
	C3–N4	28.4		21.8	11.6	8.5
1H$^+$	O1–C2	68.6	304.1	18.6	3.0	3.0
	C2–C3	44.4		31.6	19.3	16.2
	C3–N4	12.4		12.8	7.5	3.9
2	O1–C2	19.8	352.1	18.9	10.7	7.3
	C2–C3	28.3		33.0	22.5	19.4
	C3–C4	31.6		33.1	22.3	19.1
	C4–N5	27.3		21.9	11.9	8.8
2H$^+$	O1–C2	81.4	333.4	18.6	2.5	2.5
	C2–C3	70.5		33.2	15.8	15.8
	C3–C4	52.0		33.7	17.6	17.6
	C4–N5	14.2		14.5	8.3	4.7
3	O1–C2	18.5	391.8	19.0	11.0	7.6
	C2–C3	33.0		33.4	22.5	18.1
	C3–C4	24.3		36.6	27.0	23.7
	C4–C5	36.3		33.6	22.1	18.9
	C5–N6	29.3		21.9	11.6	8.5
3H$^+$	O1–C2	90.0	368.8	18.7	2.3	2.3
	C2–C3	87.0		34.0	15.8	15.8
	C3–C4	61.0		37.0	20.2	20.2
	C4–C5	47.0		34.2	18.5	18.5
	C5–N6	12.2		14.6	9.0	5.3

[a] Potential energy barrier of the internal rotation around the "bond"; value in kJ mol^{-1}, calculated at the HF/6-31G(d) level.
[b] Total entropy (J K^{-1} mol^{-1}) of the species considered calculated using the Pitzer's procedure for the torsional modes.
[c] Contribution to the entropy of the torsional modes calculated using the Pitzer's method or within the harmonic oscillator or rigid free rotor approximations.

transition structures are eclipsed conformers in which the internal hydrogen bond is clearly broken. By contrast, the rotation of the NH_3 group around the C3–N4 bond presents a barrier height of only 12 kJ mol^{-1} and a three-fold symmetry. This low energy barrier is due to the fact that the NH_3 group can rotate whilst maintaining one (or two) favorable interactions between one (or two) H of the NH_3 group and the lone pair of the oxygen atom. No complete breaking of the internal hydrogen bond is thus, occurring during the rotation around the C3–N4 bond.

Microwave spectrum of 1,3-aminopropanol, **2**, has been interpreted by the existence of an internal hydrogen bond of the type OH···N at room temperature [29]. Indeed, molecular orbital calculations confirm that the most stable conformation of **2** presents this kind of intramolecular interaction in a chair arrangement including the bonding hydrogen and the five heavy atoms [28c,29b] (**2**gG'Gg', Fig. 7). The OH···N bond energy may be estimated to16 kJ mol^{-1} and the energy barriers associated with the CC or CN torsional modes, which are close to 30 kJ mol^{-1}, clearly include the breaking of this hydrogen bond. It is not the case for the rotation around the C–O bond because the OH···N bond cleavage is partly compensated by the formation of a NH···O bond (the stable conformer containing this arrangement is situated 14 kJ mol^{-1} above **2**gG'Gg'). This explain why the corresponding critical energy amounts for only ∼20 kJ mol^{-1}. After protonation, the rotational

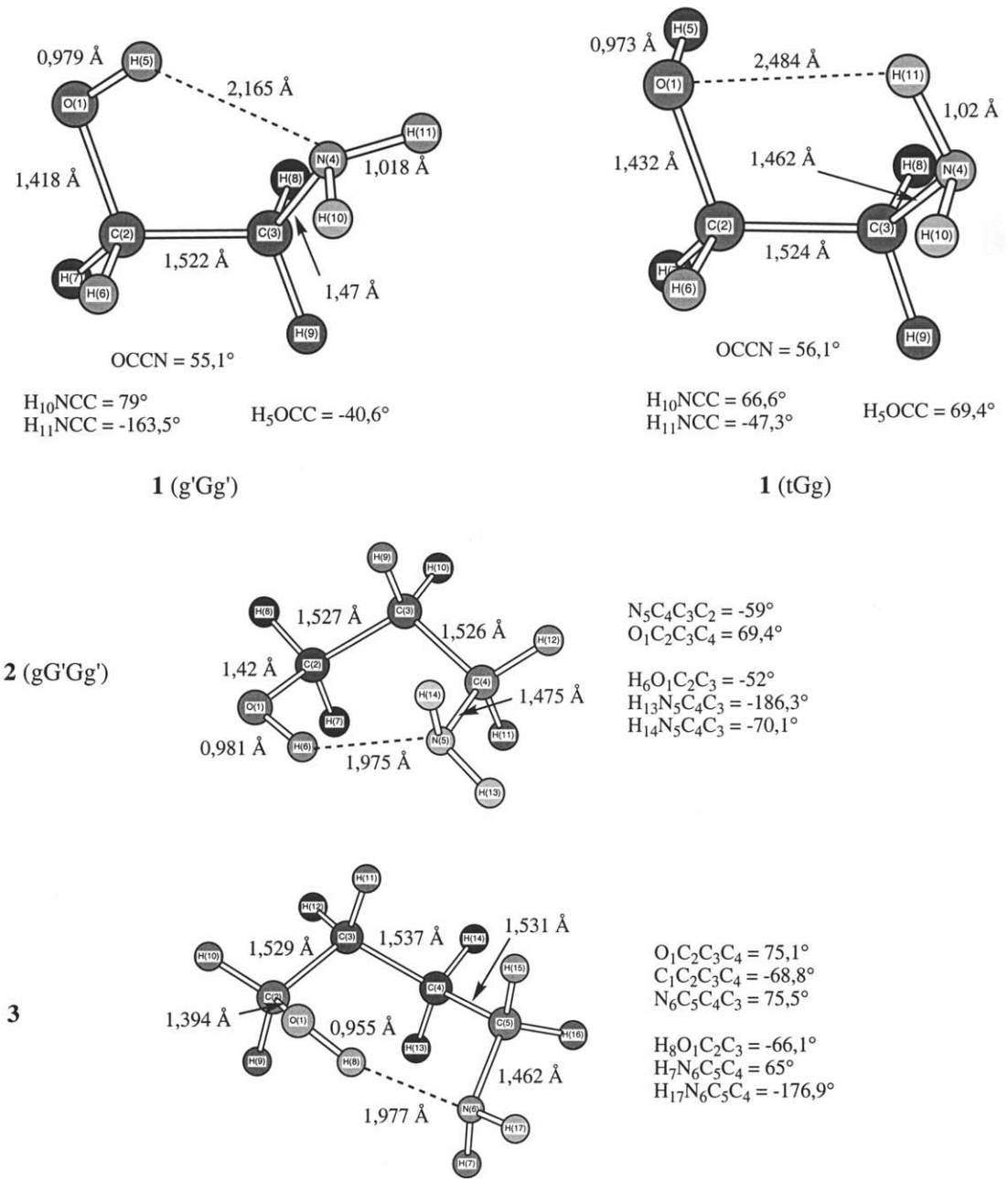

Fig. 7. MP2/6-31G(d) optimized geometry of the most stable conformers of neutral aminoalcohols **1**–**3** (bond lengths in Å, bond angles in °).

barriers are considerably increased except for the C–N bond. This phenomenon has the same origin as that evidenced for protonated 1,2-aminoethanol, **1H**$^+$: the rotation of the NH_3 group preserves an internal hydrogen bonding, thus, reducing the rotational barrier.

The most stable form of 1,4-aminobutanol, **3**, presents also a OH···N hydrogen bond in a pseudo-chair conformation (Fig. 7). The hydrogen bond energy may be estimated to ca. 20 kJ mol^{-1}, an amount of energy recovered in the rotational critical energies except for the C–O bond, as already observed for **2**. Not surprisingly, The rotational barriers are significantly increased in the protonated molecule, **3H**$^+$, with the exception of that corresponding to the C–N bond.

Calculation of the contributions to S° of the torsional modes by the Pitzer's method uses corrective terms which are dependent upon the rotational barrier height V_0 [27]. When this barrier exceeds ca. 50 kJ mol^{-1} (i.e., 20RT at 298 K), the S° term is close to that which is calculated using the harmonic oscillator approximation. For the neutral aminoalcohols **1**–**3**, the rotational barrier height is situated between 18 and 36 kJ mol^{-1} and the use of the Pitzer's approach was necessary to estimate S°(M) at 298 K. In the case of the protonated species, **1H**$^+$–**3H**$^+$, the rotational barriers are generally larger than 50 kJ mol^{-1} and the harmonic oscillator approximation has been found to correctly work. As observed above, the only exception is the rotation of the NH_3 group which may occur without a complete breaking of the internal hydrogen bond. For this latter torsional mode, the rotational barrier is situated between 12 and 14 kJ mol^{-1} and the symmetry number is equal to 3. In that case again, the Pitzer's method has been used to estimate its entropic participation. The individual contributions to entropy of each torsional modes, S°_t, estimated following the Pitzer model and the harmonic oscillator and free rotor approximations are presented in Table 11. The entropy differences $\Delta S^\circ_p = S^\circ(MH^+) - S^\circ(M)$, calculated using this procedure are presented in Table 12.

As expected, most of the entropy differences ΔS°_p is coming from the entropy terms associated with the internal rotations. Considering the rotations which are hindered after the protonation, for the three investigated molecules, each individual contribution to ΔS°_p falls in the range -4 to -7 J K^{-1} mol^{-1}. This entropy loss is obviously related to the large increase of the rotational barrier when passing from the neutral to the protonated structures. The contribution to the entropy difference ΔS°_p associated with the rotation of the amino group bearing the proton is close to a common value of -4 J K^{-1} mol^{-1}. A negative value may be surprising since the corresponding rotational barriers decreases from the neutral to the protonated forms, however a major contribution to ΔS°_p is due to the symmetry change of this torsional mode during protonation. The net result is a clear decrease of the entropy difference ΔS°_p when the size of the molecule increases in qualitative agreement with the experimental observations [22]. However, the comparison between the calculated and experimental entropy differences ΔS°_p (Table 12) is disappointing. If a correct agreement is observed for **1** (calculated

Table 12
Protonation thermochemistry of aminoalcohols **1**–**3**

	H°_{298} (Hartree)[a]	$\Delta_f H^\circ_{298(calc)}$ (kJ mol^{-1})[a]	PA(M) (kJ mol^{-1})[a]	ΔS°_p (J K^{-1} mol^{-1})[b,d]	GB(M) (kJ mol^{-1})[c,d]
1	−210.02220	−219.6	921.8 (930.3)	−8.0 (−3.3)	887.0 (896.8)
1H$^+$	−210.368968	394.5	–	–	–
2	−249.244436	−236.6	950.6 (963.6)	−18.7 (−44.2)	914.8 (917.9)
2H$^+$	−249.604157	343.4	–	–	–
3	−288.468285	−257.8	962.5 (984.0)	−23.0 (−65.4)	925.1 (932.0)
3H$^+$	−288.832526	310.5	–	–	–

[a] Calculated G2(MP2) results.
[b] $\Delta S^\circ_p = S^\circ(MH^+) - S^\circ(M)$; $S^\circ(MH^+)$ and $S^\circ(M)$ values are presented in Table 11.
[c] Calculated using $GB(M) = PA(M) - T[\Delta S^\circ_p - S^\circ_{H^+}]$.
[d] In parentheses, experimental determinations from [24], adjusted to the most recent basicity scale [23].

$\Delta S^\circ_p = -8.0\,J\,K^{-1}\,mol^{-1}$ compared with the experimental value of $-3.3\,J\,K^{-1}\,mol^{-1}$), the deviation attains 25 and $42\,J\,K^{-1}\,mol^{-1}$ for **2** and **3**, respectively. This difference is far from the estimated error of $0.5\,J\,K^{-1}\,mol^{-1}$ per rotation assumed on the S° calculated using the Pitzer's tables. Moreover, the maximum contribution to ΔS°_p corresponding to the hindrance of one internal rotation may be estimated by considering the S°_t term calculated using the harmonic oscillator for the protonated species and that calculated using the free rotor for the neutral. Using the data of Table 11, we calculate a difference of ca. $16\,J\,K^{-1}\,mol^{-1}$ per rotation. This means that the ΔS°_p values cannot decrease by more than $16\,J\,K^{-1}\,mol^{-1}$ when passing from **1** to **2** and **3**; the experimentally derived values, 41 and $21\,J\,K^{-1}\,mol^{-1}$ are thus, probably too high. Finally, one may note that significant discrepancies have been already observed in the experimental determination of ΔS°_p from one laboratory to another [15b,24] and that better agreement is obtained when comparing Gibbs free energy changes.

It has been recalled in the computational section that G2 methods may provide accurate estimate of the proton affinities. The proton affinities values quoted in Table 12 have been calculated using the G2(MP2) H_{298} values for M and MH^+ and the enthalpy of translation of the proton ($6.2\,kJ\,mol^{-1}$). Examination of Table 12 shows that the calculated proton affinity values are systematically lower than the experimental ones. The deviations (8.5, 13.0 and $21.5\,kJ\,mol^{-1}$ for **1**, **2** and **3**, respectively) are significantly higher than that expected with G2(MP2) calculations ($\pm 6\,kJ\,mol^{-1}$) [20d]. Curiously, the deviation seems to increase with the size of the molecule. Since the proton affinity value is dependent on the choice of the ΔS°_p values used in the expression $PA(M) = GB(M) + T\,[\Delta S^\circ_p - S^\circ H^+]$, these observation suggests that the experimental ΔS°_p (values into parentheses in Table 12) are too negative, and that this phenomenon increases when passing from **1** to **3**. Combining the calculated proton affinities and ΔS°_p values, theoretical gas-phase basicity estimates may be proposed. The GB(M) obtained by this means are compared with the experimental values in Table 12. It can be seen that the calculated GB values are again lower than the experimental values, but, that time, the mean difference amounts for only $6.6\,kJ\,mol^{-1}$ for the three compounds **1**, **2** and **3**. This better agreement between the calculated and experimental gas phase basicities speaks again for ΔS°_p values closer to that estimated here using the Pitzer's method than to that derived from experiments.

3.6. Stereochemical effects during the dissociation of protonated 1,2-aminoalcohols

We return now to the question, raised by Pierre Longevialle and recalled in Section 1: how to explain the influence of the OCCN dihedral angle upon the protonation energetics of 1,2-aminoalcohols and on the dehydration efficiency of their protonated forms? To answer this question, we have examined the MP2/6-31G(d) potential energy of 1,2-aminoethanol, **1**, and its oxygen and N-protonated forms as a function of the dihedral angle OCCN, θ.

The potential energy curve associated with the neutral molecule **1** (Fig. 8, top) presents two minima at $\theta = \pm 55.1^\circ$ corresponding to the two enantiomeric conformers g'Gg' (see Fig. 7). As expected the inversion barrier ($\theta = 0^\circ$, $23\,kJ\,mol^{-1}$) is lower than the energy required to break the internal hydrogen bond in order to generate the *trans* conformer ($\theta = 125^\circ$, $34\,kJ\,mol^{-1}$). A comparable potential energy curve is observed for the N-protonated form $\mathbf{1H}^+$ (Fig. 8, bottom). The critical energies are however, different according to the stronger internal hydrogen bond in this species (18 and $49\,kJ\,mol^{-1}$, respectively). Obviously, the difference between the two potential energy curves of **1** and the N-protonated form of $\mathbf{1H}^+$ is the reflect of the proton affinity shift, ΔPA, induced by the freezing of the dihedral angle θ. The evolution of ΔPA with θ, as calculated from the MP2/6-31G* results, is presented in Fig. 9.

From $\theta = -50^\circ$ to $\theta = 50^\circ$, the proton affinity is practically constant and a clear decrease of the proton affinity is observed when θ exceeds 50°, i.e., when, increasingly, the internal hydrogen bond is broken. For the purpose of comparison, the experimental ΔPA values obtained by Houriet et al. [4] for the series

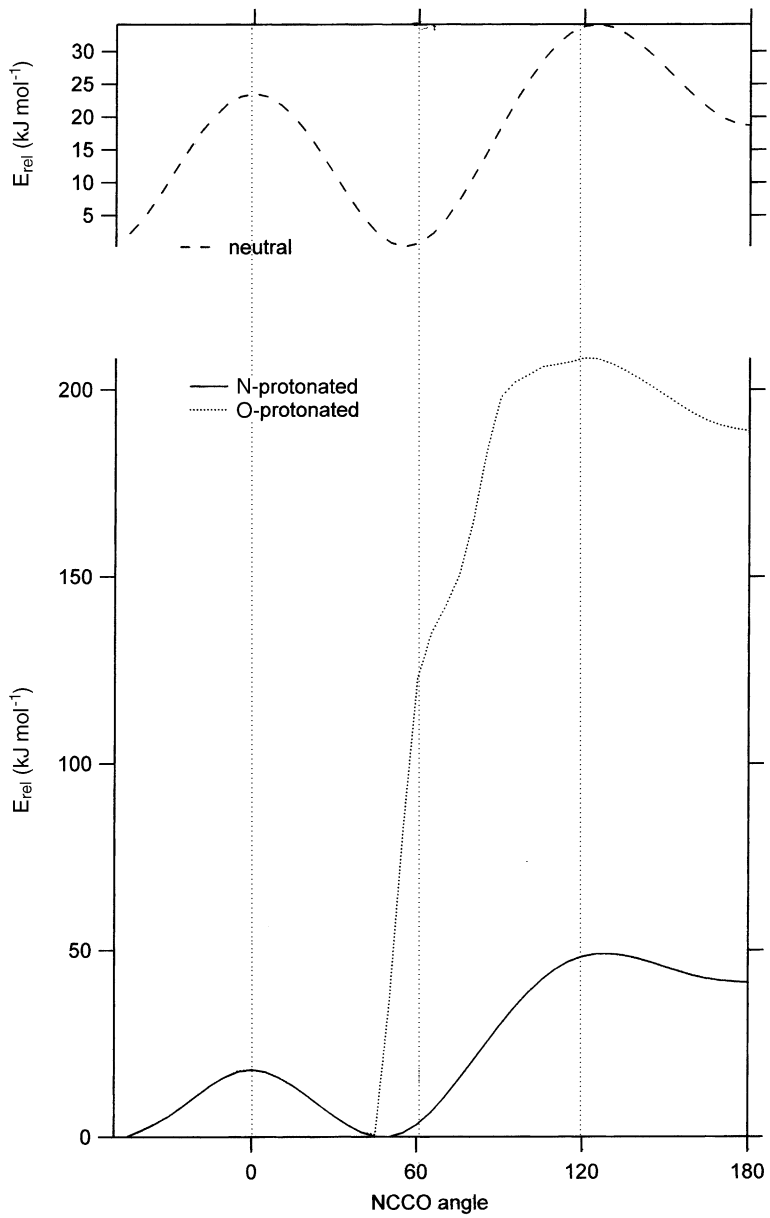

Fig. 8. Calculated MP2/6-31G(d) potential energy of neutral and protonated 1,2-aminoethanol as a function of the dihedral angle NCCO.

of α,β-aminoalcohols studied by Pierre Longevialle are also indicated in Fig. 9. The excellent agreement between the two sets of data, thus, confirms that the experimentally observed ΔPA is essentially the reflect of the difference in the internal hydrogen bond in the neutral and the protonated molecule.

Fig. 8 presents also the potential energy curve associated with the O-protonated form of **1**. Note that, for $\theta = 180^{\circ}$, the corresponding structure is simply the $\mathbf{1C_1}$–**N** form described in Fig. 1. As indicated in Fig. 8, the potential energy of the O-protonated molecule slightly increases when decreasing θ from

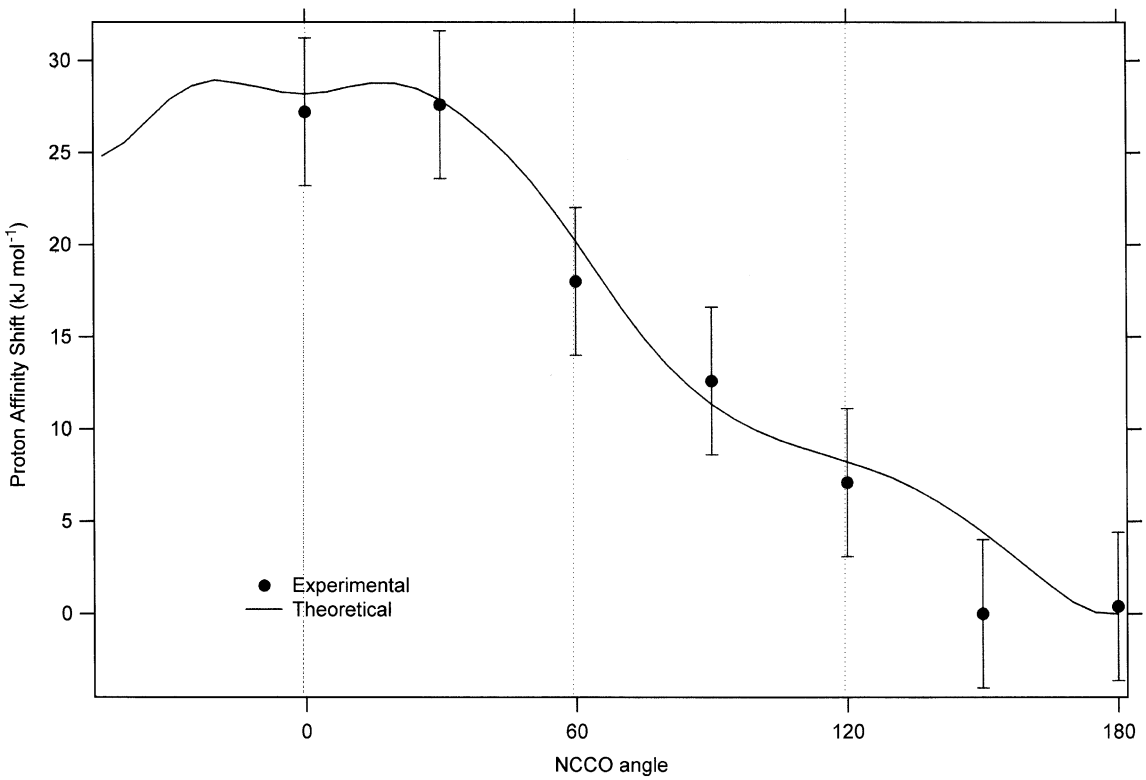

Fig. 9. Calculated MP2/6-31G(d) proton affinity variation of 1,2-aminoethanol as a function of the dihedral angle NCCO (the experimental points are from [4]).

180 to 120° and further decreases gently to $\theta \sim 90°$. Below this dihedral angle value, the potential energy falls dramatically and, near $\theta = 60°$, the O-protonated structure becomes unstable and the system suddenly evolves toward the N-protonated form. Thus, the O-protonated form of **1** is stable only between $\theta \sim 60°$ and $\theta = 180°$. In addition to this limitation, the water loss efficiency is expected to be the reflect of the geometrical constraints on the corresponding transition structure. For $\theta = 180°$, the atoms arrangement is optimum for the elimination of the water molecule via the internal nucleophilic substitution reaction as described in the preceding part. When reducing the angle θ, it becomes difficult for the nitrogen atom to approach the vicinal carbon atom back to the OH_2 group. When $\theta = 120°$, this backside attack is obviously forbidden and if θ is further reduced, the most favorable reaction becomes the proton migration from the oxygen to the nitrogen atom rather than the switching to the second possible mechanism of water loss, i.e., the 1,2-hydride shift. The calculation thus predicts an efficient loss of water from the O-protonated form of α,β-aminoalcohols for dihedral angles situated between 180 and 120°. This is exactly what has been observed by Longevialle et al. [2] and perfectly in line with his interpretation.

4. Conclusion

The present study demonstrates that protonated α,ω-aminoalcohols present a behavior more contrasted than previously assumed. Collisional experiments show that the structure of the low energy

dissociation products are always that expected from the internal nucleophilic substitution reactions. For 1,2- and 1,3-aminoalcohols, this reaction corresponds to the water loss while for 1,4- and 1,5-aminoalcohols it corresponds to ammonia loss. Clearly, these observations are not directly related to the endothermicity of the reactions. Molecular orbital calculations demonstrate that the intramolecular nucleophilic substitution reactions proceed via two intermediate structures (***n***C_1 –**N** and ***n***C_2–**N** for the water loss and ***n***C_1–**O** and ***n***C_2–**O** for the ammonia loss). This situation is reminiscent of the double wells potential energy surface associated with intermolecular S_N2 reactions involving cationic substrates (see for example [30]) or intramolecular nucleophilic substitution reactions accompanying the elimination of water or ammonia from protonated diols [14] or diamines [25]. A major observation is that the formation of the structure ***n***C_1–**N**, where the proton is localized on the oxygen atom, needs 180–200 kJ mol^{-1}. This reaction is thus, observed only for 1,2- and 1,3-aminoalcohols **1** and **2** because all the other possible dissociation routes have critical energies higher than 220–250 kJ mol^{-1}. In contrast, protonated 1,4- and 1,5-aminoalcohols **3** and **4** eliminate quasi-exclusively ammonia since the corresponding critical energies are in the 150–170 kJ mol^{-1} range.

A detailed conformational analysis of both the neutral and the protonated forms of **1**–**3** lead us to propose theoretical values for the thermochemical quantities associated with the protonation process. Good agreement with experiment is found between gas phase basicities but significant discrepancies are observed for proton affinities and protonation entropies. Finally, the stereochemical effects observed on the proton affinity of conformationally blocked 1,2-aminoalcohols and on the dissociation of their protonated forms has been illustrated and discussed using **1** as a suitable model.

References

[1] P. Longevialle, G.W.A. Milne, H.M. Fales, J. Am. Chem. Soc. 95 (1973) 6666.

[2] P. Longevialle, J.P. Girard, J.C. Rossi, M. Tichy, Org. Mass Spectrom. 14 (1979) 414.

[3] P. Longevialle, J.P. Girard, J.C. Rossi, M. Tichy, Org. Mass Spectrom. 15 (1980) 268.

[4] R. Houriet, H. Rüfenacht, P.A. Carrupt, P. Vogel, M. Tichy, J. Am. Chem. Soc. 105 (1983) 3417.

[5] M. Bensimon, J. Rapin, R. Houriet, Spectrosc. Int. J. 3 (1984) 145.

[6] R. Houriet, H. Rufenacht, D. Stahl, M. Tichy, P. Longevialle, Org. Mass Spectrom. 20 (1985) 300.

[7] H.E. Audier, A. Milliet, C. Perret, J.C. Tabet, P. Varenne, Org. Mass Spectrom. 13 (1978) 315.

[8] D.V. Davis, R.G. Cooks, Org. Mass Spectrom. 16 (1981) 17.

[9] V.H. Wysocki, D.J. Burinsky, R.G. Cooks, J. Org. Chem. 50 (1985) 1287.

[10] J.S. Brodbelt, V.H. Wysocki, R.G. Cooks, Org. Mass Spectrom. 23 (1988) 54.

[11] E.S. Eichmann, J.S. Brodbelt, Org. Mass Spectrom. 28 (1993) 665.

[12] E.S. Eichmann, J.S. Brodbelt, J. Am. Soc. Mass Spectrom. 4 (1993) 230.

[13] T. Partanen, P. Vainiotalo, G. Stajer, G. Bernath, K. Pihlaja, Org. Mass Spectrom. 29 (1994) 126.

[14] G. Bouchoux, N. Choret, R. Flammang, J. Phys. Chem. 101 (1997) 4271.

[15] (a) G. Bouchoux, N. Choret, F. Berruyer-Penaud, J. Phys. Chem. 105 (2001) 3989;
(b) G. Bouchoux, N. Choret, F. Berruyer-Penaud, R. Flammang, J. Phys. Chem. 105 (2001) 9166.

[16] J.L. Holmes, A.D. Osborne, Int. J. Mass Spectrom. Ion Processes 23 (1977) 189.

[17] R.H. Bateman, J. Brown, M. Lefevere, R. Flammang, Y. Van Haverbeke, Int. J. Mass Spectrom. Ion Processes 115 (1992) 205.

[18] Gaussian-98, Revision A.6, M.J. Frisch, G.W. Trucks, H.B. Schlegel, G.E. Scuseria, M.A. Robb, J.R. Cheeseman, V.G. Zakrzewski, J.A. Montgomery Jr., R.E. Stratmann, J.C. Burant, S. Dapprich, J.M. Millam, A.D. Daniels, K.N. Kudin, M.C. Strain, O. Farkas, J. Tomasi, V. Barone, M. Cossi, R. Cammi, B. Mennucci, C. Pomelli, C. Adamo, S. Clifford, J. Ochterski, G.A. Petersson, P.Y. Ayala, Q. Cui, K. Morokuma, D.K. Malick, A.D. Rabuck, K. Raghavachari, J.B. Foresman, J. Cioslowski, J.V. Ortiz, B.B. Stefanov, G. Liu, A. Liashenko, P. Piskorz, I. Komaromi, R. Gomperts, R.L. Martin, D.J. Fox, T. Keith, M.A. Al-Laham, C.Y. Peng, A. Nanayakkara, C. Gonzalez, M. Challacombe, P.M.W. Gill, B. Johnson, W. Chen, M.W. Wong, J.L. Andres, C. Gonzalez, M. Head-Gordon, E.S. Replogle, J.A. Pople, Gaussian, Inc., Pittsburgh, PA, 1998.

[19] P. Scott, L. Radom, J. Phys. Chem. 100 (1996) 16502.

[20] (a) L.A. Curtiss, K. Raghavachari, G.W. Trucks, J.A. Pople, J. Chem. Phys. 94 (1991) 7221;
(b) L.A. Curtiss, K. Raghavachari, J.A. Pople, J. Chem. Phys. 98 (1993) 1293;
(c) L.A. Curtiss, P.C. Redfern, B.J. Smith, L. Radom, J. Chem. Phys. 104 (1996) 5148;
(d) L.A. Curtiss, K. Raghavachari, P.C. Redfern, J.A. Pople, J. Chem. Phys. 106 (1997) 1063;

(e) A. Nicolaides, A. Rauk, M.N. Glukhovtsev, L. Radom, J. Phys. Chem. 100 (1996) 17460.
[21] S.G. Lias, J.E. Bartmess, J.F. Liebman, J.L. Holmes, R.D. Levin, W.G. Mallard, Gas phase ion and neutral thermochemistry, J. Phys. Chem. Ref. Data 17 (Suppl. 1) (1988).
[22] S.W. Benson, Thermochemical Kinetics, 2nd Edition, Wiley, New York, 1976.
[23] E.P.L. Hunter, S.G. Lias, J. Phys. Chem. Ref. Data 27 (1988) 413.
[24] M. Meot-Ner (Mautner), P. Hamlet, E.P. Hunter, F.H. Field, J. Am. Chem. Soc. 102 (1980) 6393.
[25] M. Meot-Ner (Mautner), J. Am. Chem. Soc. 106 1984 1257.
[26] (a) A.L.L. East, L. Radom, J. Chem. Phys. 106 (1997) 6655; (b) A.L.L. East, B.J. Smith, L. Radom, J. Am. Chem. Soc. 119 (1997) 9014.
[27] K.S. Pitzer, W.D. Gwinn, J. Chem. Phys. 10 (1942) 428.
[28] (a) Y.-P. Chang, T.-M. Su, T.-W. Li, I. Chao, J. Phys. Chem. A 101 (1997) 6107;
(b) A.M. Kelterer, M. Ramek, R.F. Frey, M. Cao, L. Schäfer, J. Mol. Struct. Theochem. 310 (1994) 45;
(c) A.M. Kelterer, M. Ramek, J. Mol. Struct. Theochem. 232 (1991) 189;
(d) L.G. Vanquickenborne, B. Coussens, C. Verlinde, C. de Ranter, J. Mol. Struct. Theochem. 201 (1989) 1;
(e) C. Van Alsenoy, K. Siam, J.D. Ewbank, L. Schäfer, J. Mol. Struct. Theochem. 136 (1986) 77.
[29] (a) M.A. McMahan, S.D. Sharma, R.F. Curl Jr., J. Mol. Spectrosc. 75 (1979) 220;
(b) A.-M. Kelterer, M. Flock, M. Ramek, J. Mol. Struct. Theochem. 276 (1992) 35.
[30] G. Bouchoux, N. Choret, Rapid Commun. Mass Spectrom. 11 (1997) 1799, and references cited therein.